bushfire&natural
HAZARDSCRC

REPORT ON FRAGILITY CURVES FOR LIMITED DUCTILE REINFORCED CONCRETE BUILDINGS

Elisa Lumantarna, Helen Goldsworthy, Nelson Lam
Department of Infrastructure Engineering, The University of Melbourne, VIC
Hing-Ho Tsang, Emad Gad, John Wilson
Department of Infrastructure Engineering, The University of Melbourne, VIC

THE UNIVERSITY
of ADELAIDE

THE UNIVERSITY OF
MELBOURNE

SWIN
BUR
NE

SWINBURNE
UNIVERSITY OF
TECHNOLOGY

Version	Release history	Date
1.0	Initial release of document	4/12/2017

Australian Government

Department of Industry, Innovation and Science

Business
Cooperative Research
Centres Programme

TABLE OF CONTENTS

ABSTRACT

FRAGILITY CURVES FOR LIMITED DUCTILE REINFORCED CONCRETE BUILDINGS

Elisa Lumantarna, *Department of Infrastructure Engineering, The University of Melbourne, VIC*

Reinforced concrete buildings make up the majority of Australian building stocks. Structural elements of these buildings are often designed with limited to nonductile detailing. With a very low building replacement rate many of the Australian buildings are vulnerable to major earthquakes and pose significant risk to lives, properties and economic activities.

Related Earthquake Risk" under the Bushfire and Natural Hazards Cooperative Research Centre (BNHCRC) aims to develop knowledge to facilitate evidence-based informed decision making in relation to the need for seismic retrofitting, revision of codified design requirement, and insurance policy. Seismic vulnerability assessment is an essential component in the project.

This report presents sets of fragility curves that have been developed for two types of reinforced concrete buildings, buildings that are mainly supported by shear or core walls and buildings that are supported by walls and moment resisting frames. The seismic assessment frameworks, the approach for selection of ground motions and the development of archetype building models will be discussed. The fragility curves for low-rise, mid-rise and high-rise buildings for both types of limited ductile reinforced concrete buildings will be presented in the forms of PGV, MMI and RSD_{max} as intensity measures.

INTRODUCTION

The project "Cost-Effective Mitigation Strategy Development for Building Related Earthquake Risk" under the Bushfire and Natural Hazards Cooperative Research Centre (BNHCRC) aims to develop knowledge to facilitate evidence-based informed decision making in relation to the need for seismic retrofitting, revision of codified design requirement, and insurance policy. Seismic vulnerability assessment is an essential component in the project.

Cost-benefit analysis will be used as a standard tool to facilitate informed decision making [1]. Apart from developing socio-economic loss models which are relevant to costing, seismic structural analysis is a core part of the project for investigating the vulnerability of different forms of structures.

This report presents sets of fragility curves which are essential inputs to cost-benefit analysis. Fragility curves will be presented for limited-ductile reinforced concrete (RC) buildings typical of Australian constructions: i) fragility curves for RC buildings that are primarily supported by limited-ductile RC shear wall (referred to **RC shear walls buildings** herein); ii) fragility curves for RC buildings that are supported by limited-ductile RC walls and frames (referred to **RC frames buildings** herein). The information presented in this report are based on the up to date knowledge of the project team. It is noted that there are ongoing works on this topic, being carried by in conjunction with PhD students who are financially supported by this BNHCRC project.

FRAMEWORK FOR SEISMIC ASSESSMENT

SEISMIC FRAGILITY FUNCTIONS

Seismic fragility functions define the building's probability of exceeding a damage limit state as a function of ground motion intensity measure (IM). In its most common form it is defined by the lognormal cumulative distribution function [2] given in Eq. (1). Hence, it is assumed that the relationship between the seismic demand (D) and the structural capacity (C) is normally distributed. This has been proven to be a reasonable assumption by numerous studies as discussed in [3].

$$P[D > C|IM] = \phi \frac{\ln(S_D/S_C)}{\beta} \tag{1}$$

Where ϕ is the standard normal cumulative distribution function

         S_C is the median value of the structural limit state (i.e. the capacity of the structural limit state)

         S_D is the median value of the demand as a function of IM

         β is the logarithmic standard deviation of IM

The fragility function expressed in Eq. (1) is suitable when the engineering demand parameter (EDP) used to assess the performance of the buildings is not dependent on individual component capacities. In this study, the performance levels for the buildings are based on when the first component in a building reaches a structural damage limit or when the inter-storey drift demand exceeds the inter-storey drift limits. The EDP adopted in this study is the critical demand-to-capacity ratio (Y) which corresponds to the component response or inter-storey drift that will first cause the building to reach the performance limit. The fragility function for which the engineering demand parameter is the critical demand-to-capacity ratio is provided in Eq. (2). Furthermore, Eq. (2) also incorporates aleatoric and epistemic uncertainties within the fragility function.

$$P[Y > 1|IM] = \phi \frac{\ln(\eta_{Y|IM})}{\sqrt{\beta_{Y|IM}^2 + \beta_C^2 + \beta_M^2}} \tag{2}$$

Where $\eta_{Y|IM}$ is the median critical demand-to-capacity ratio as a function IM

         $\beta_{Y|IM}$ is the dispersion (logarithmic standard deviation) of the critical demand-to-capacity ratio as a function of IM

         $\beta_{D|IM}$ dispersion of the demand as a function of IM

         β_C is the capacity uncertainty

         β_M is the modelling uncertainty

Aleatoric uncertainties are caused by factors that are inherently random in nature, whereas epistemic uncertainties are knowledge-based due to assumptions and modelling limitations and hence may be reduced with improved knowledge and modelling methods [4]. The aleatoric uncertainty

related to the demand (as a function of IM), $\beta_{D|IM}$ is calculated based on the seismic analysis results. The dispersion related to the uncertainty of determining the capacity of structural components, β_C (aleatoric uncertainty) and the dispersion due to modelling uncertainties, β_M (epistemic uncertainty) are usually computed based on recommendations provided by other studies and guidelines [5–7]. In this study the dispersion associated with modelling uncertainty (β_M) is set to 0.2 based on recommendations provided by FEMA-P695 [8]. The dispersion related to uncertainty in predicting the capacity of components (β_C) is conservatively set to 0.3.

PROBABILISTIC SEISMIC DEMAND MODEL

To compute the fragility function, it is first necessary to develop a probabilistic seismic demand model (PSDM) which relates the engineering demand parameter (in this study, the critical demand-to-capacity ratio) to the intensity measure. There are various procedures used to obtain the PSDM; the well-established methods which are obtained through conducting dynamic nonlinear time-history analysis (THA) are incremental dynamic analysis [9], multiple stripe analysis [10 and cloud analysis [11].

RC shear walls buildings

The multiple stripe analysis MSA approach was adopted for the construction of fragility curves of RC shear wall buildings. The multiple stripe analysis (MSA) involves conducting multiple time history analyses for a discrete set of IM and for each IM a different suite of ground motion records is selected [10]. The method is commonly used when the ground motion properties change for each IM, for example when the conditional spectrum method is used to select ground motions [3]. Hence, the method can provide the most accurate results especially if unscaled records are used for each intensity measure. Due to the inherent variability of the records used at different intensities, the response obtained from the time history analyses may not necessarily result in an increase of the fraction of responses exceeding the damage limit state with increasing level of IM. Furthermore, unlike incremental dynamic analysis, MSA does not require the analyses to be conducted up to an IM for which all of the records cause the building response to exceed the damage limit state.

The method of calculating fragility curves using the MSA approach is given in Baker [3], where the logarithm likelihood function has been maximized and expressed in the form of Eq. (3) to obtain the parameters defining the fragility functions (Eq. (2)). It should be noted that a binominal distribution is used to calculate the probability of observing the number z_j the performance limits has been exceeded out of n_j ground motions.

$$\{\widehat{\eta_{Y|IM}}, \hat{\beta}\} = \arg\max(\eta_{Y|IM}, \beta) \sum_{j=1}^{m} \left\{ \ln\binom{n_j}{p_j} + z_j \ln \sigma\left(\frac{\ln(\eta_{Y|IM})}{\beta}\right) + (n_j - z_j) \ln\left(1 - \sigma\left(\frac{\ln(\eta_{Y|IM})}{\beta}\right)\right) \right\} \quad (3)$$

where p_j is the 'probability that a ground motion with *IM* will cause a performance limit of structures to be exceeded and *m* is the number of *IM* levels.

RC frames buildings

The cloud analysis involves using unscaled records to obtain a cloud of intensity-response data points. Regression analysis is conducted for the cloud of data to approximate the fragility function parameters. The method requires significantly less THA since multiple analyses at a certain IM is not necessary. However, record selection plays a key role on the accuracy of the method and it is recommended that the suite of records selected cover a wide range of IM and that a significant portion of the records provide data points near the damage limit state (i.e. for this study when Y=1) [12,13]. Furthermore, unscaled records must be used. For the same set of analyses different IMs may be selected to obtain different PSDM and from the regression analyses it is possible to select the best IM to represent the demand quantity [13]. The cloud analysis assumes a constant conditional standard deviation for the probability distribution of the engineering demand parameter given IM [14]. The engineering demand model takes the form of a power-law expressed by Eq. (4) [15]:

$$\eta_{Y|IM,50\%} = a.IM^b \tag{4}$$

Where $\eta_{Y|IM,50\%}$ is the conditional median demand-to-capacity ratio parameter

              $a \ and \ b$ are the parameters obtained from regression analysis

Furthermore, since the parameters $\eta_{Y|IM}$ and $\beta_{Y|IM}$ obtained using the cloud analysis method are based on the correlation of the structural response to a given intensity measure, it may be necessary to separate the results obtained from the analyses which have encountered numerical instabilities. This is particularly important when evaluating the response of nonlinear building models up to the point of collapse since it is likely for numerical instabilities to take place for stronger ground motion records. Therefore the fragility function used by Rajeev et al. [16] expressed by Eq. (5) has been adopted, where the *collapse* (c) and *non-collapse* ($\bar{c}$) case are separated. It is noted that *collapse* cases do not necessarily refer to the definition of collapse for a building or exceedance of a performance level (i.e. in this study when Y > 1.0); instead, it refers to cases for which the results are considered to be unreliable due to numerical instabilities or the performance level has been exceeded by a significant amount. Furthermore, since in this study four different performance levels are investigated, it is expected that Y will be significantly greater than 1.0 for performance levels corresponding to lower level of damage. Thus, limits defining *collapse* cases should be carefully defined for each performance level.

$$P(Y > 1|IM) = P(Y > 1|IM, \bar{c}).[1 - P(c|IM)] + P(c|IM) \tag{5}$$

Where

            c is the collapse situation

            $\bar{c}$ is the non-collapse situation

            $P(Y > 1|IM, \bar{c})$ is provided in Eq. (6)

            $P(c|IM)$ is provided in Eq. (7)

$$P(Y > 1|IM, \bar{c}) = \frac{\ln(\eta_{Y|IM,\bar{c}})}{\sqrt{\beta_{Y|IM,\bar{c}}^2 + \beta_C^2 + \beta_M^2}} \tag{6}$$

$$P(c|IM) = \frac{no.\,of\,records\,causing\,collapse}{total\,no.\,of\,records} \tag{7}$$

PERFORMANCE LEVELS

There are many different performance levels which are defined in the literature and codes, each with different acceptance criteria. The following section provides a review of the performance limits defined in the literature and codes, and the proposed limits for this study are presented. Since there are numerous terminologies used to define various performance limits, the section below provides a review for four general damage limits: (i) slight damage, (ii) moderate damage, (iii) extensive damage, and (iv) complete damage.

Slight damage

Performance limits that typically fall within the Slight Damage criteria are: Operational, Serviceability, and Immediate Occupancy.

The *Operational* or *Serviceability* limit state essentially refers to a limit state for which the structure remains operational after an earthquake, and hence the damage (if any) is very minor. This damage state corresponds to the building elements remaining elastic or close to elastic.

Priestley et al. [17] define the *Serviceability* limit by proposing strain limits. They state that the compression strain limit at this limit should be a "conservative estimate of the strain at which spalling initiates" and suggest a compression strain limit of 0.004. For the tensile limit state, Priestley et al. [17] argue that an 'elastic' or 'near elastic' limit is too conservative since strains of several times the yield strain can be sustained by the reinforcement without requiring repair. Instead, they state that the tensile limit should be based on limiting crack widths to approximately 1.0 mm. Based on experimental findings; they recommend tensile strain limits of 0.015 for members carrying axial load, and 0.01 for members without axial load.

ASCE/SEI 41[18] defines the *immediate occupancy* as "… post-earthquake damage state in which only very limited structural damage has occurred" and that the "… basic vertical- and lateral-force-resisting systems of the building retain almost all of their pre-earthquake strength and stiffness."

The performance limits are defined to account for the damage that may occur to non-structural components. Sullivan et al. [19] suggest limiting the maximum interstorey drift to 0.4 % for buildings with brittle non-structural elements and 0.7 % for buildings with ductile structural elements. These drift limits correspond to a performance limit defined as *No Damage*.

RC Shear walls buildings

The performance limits for slight damage adopted for RC shear wall buildings are more conservative in comparison to Priestley et al. [17] for *Serviceability* limit due to the non-ductile detailing of the walls that were assessed. A compression strain limit of 0.001 was adopted to ensure a close to elastic response for the concrete, and a tensile strain limit of 0.005 was adopted to ensure small residual crack widths.

RC frames buildings

RC walls with non-ductile detailing are likely to experience a single crack and have cracking moment capacities which are greater than the yield moment capacity. The slight damage (*serviceability*) limit is defined as when the walls reach initial yield. This is because significant increase in strains, especially in the longitudinal reinforcement bars is likely to follow shortly after initial yield is reached. For the sake of completeness, nominal yield is taken as the slight damage limit for the RC frames, although this is unlikely to govern. For non-structural damage, a maximum drift of 0.4 % is suggested as older buildings (and current buildings) are likely to have brittle non-structural components.

Moderate damage

Performance limits that typically fall within the Moderate Damage criteria are: Damage Control and Repairable Damage.

Priestley et al. [17] define the compressive strain limit at the *Damage Control* limit to correspond to when the transverse reinforcement confining the core fractures. The compressive strain limit at this limit is obtained by adding the strain-energy capacity of the confining steel to the unconfined strain energy of the concrete. For the tensile limit state, Priestley et al. [17] recommend adopting 0.6 times the ultimate tensile strain of steel obtained from monotonic tensile tests. The reduced ultimate tensile strain is suggested to account for the decrease of steel tensile strain capacity due to: cyclic loading, vulnerability of reinforcement to buckling after it has experienced tensile strains, low-cycle fatigue, slip between reinforcing steel and concrete at critical section, and tension shift effects which result in higher strains being developed in the steel than those obtained from sectional analyses which assume plane-sections. However, Priestley et al. [17] provided a limit for the spacing of transverse reinforcement hoops and ties to ensure that the level of strains is attainable without the buckling of longitudinal bars and this limit is generally much smaller than the spacing specified in AS3600:2009 [20.

Sullivan et al. [19] suggest limiting the maximum interstorey drift to 2.5 % for buildings with brittle and ductile non-structural elements, for performance limit corresponding to Repairable Damage. The New Zealand Standard, NZS 1170.5 [21] requires the drift limit to also be limited to 2.5 % for the performance limit corresponding to Damage Control. The Australian Standard, AS 1170.4 [22] requires a more conservative drift limit of 1.5 % for the Ultimate limit state. In the commentary for AS 1170.4 [23] it is explained that this drift limit is intended to "… restrict damage to partitions, shaft and stair enclosures and glazing…" as well as indirectly providing an upper bound for P-delta effects. However, it is important to note that in Australia little consideration is given to the seismic drift capacity of non-structural components. McBean [24] highlighted, based on limited

available data from manufacturers, that non-structural components (curtain walls) may reach ultimate drift conditions at displacements of 30-50 mm or less.

RC shear wall buildings

In non-ductile RC components ultimate failure occurs at compressive strains of 0.003 to 0.004, and hence significant spalling could occur which would lead to significant repair costs thus exceeding the Damage Control limit state. In addition, lower tensile strain limits than those suggested by Priestley et al. [17] are likely to be suitable for walls with low longitudinal reinforcement ratios and with longitudinal bars that are not well restrained, since they are vulnerable to having a single crack form at the base leading to strain localisation, and to buckling after high strains have been reached in tension although buckling may be less likely to occur due to the limited cracks formed.

For RC shear wall buildings, a compression strain limit of 0.002 was adopted for the moderate damage limit states to reduce the likelihood of spalling. A tensile strain limit of 0.01 was adopted to reduce the likelihood of low-cycle fatigue and out of plane buckling of the reinforcement during load reversals.

RC frames buildings

For RC frames buildings a concrete compressive strain limit of 0.002, and a tensile strain limit of 0.015, were set for the RC walls. The tensile strain limit is slight higher than that adopted for RC walls as the walls consider for this buildings have Y-bars and hence a design ultimate strain of 0.12. For the frame elements, the moderate damage limit is defined as the rotation corresponding to the point midway between the nominal yield rotation and the shear failure rotation. For non-structural damage limit, a maximum drift of 0.8 % is suggested, although it is acknowledged that further research is required for determining non-structural drift limits in Australia.

Extensive damage

The *Extensive Damage* limit usually corresponds to the *Life Safety* performance limit, which is defined in ASCE/SEI 41 [18] as the post-earthquake damage state "… in which significant damage to the structure has occurred but some margin against either partial or total structural collapse remains." ASCE/SEI 41 [18] describes the extent of this damage limit for walls to allow for some spalling and crushing, and limited buckling of bars. For non-ductile frame elements, this corresponds to limited cracking and splice failure of some columns.

RC shear wall buildings

In this study the extensive damage (*Life Safety*) performance limit essentially describes the initiation of loss of the lateral load resisting system. It corresponds to the ultimate drift capacity for the RC walls. Therefore, the compressive strain limit for the RC walls is limited to 0.004 which corresponds to the compressive strain used in this study to determine the ultimate moment capacity of wall sections. The tensile strain is limited to 0.6 times the uniform tensile strain for the reasons suggested by Priestley et al. [17] for the *Damage Control* limit, but due to the dangers associated with strain localisation in of the walls and the potential rupture of the longitudinal bars characteristic of the walls assessed in this study these strain limits are more applicable at the *Life Safety* limit.

RC frames buildings

For RC frames buildings, the strain limits for the RC walls are set to be the same as those for RC wall buildings. For the RC frames, the limits for extensive damage are set as the rotation which defines shear failure, since this corresponds to the point at which the lateral load resistance decreases.

For the non-structural elements, a maximum drift of 1.5 % is suggested for the extensive damage limit state in accordance with AS 1170.4:2007 for the *Ultimate* limit state.

Complete damage

The Complete Damage limit state is commonly referred to as the *Collapse Prevention* performance limit. In more recent studies, the point for which a building may be defined as collapsed has evolved and may be determined via various mechanisms as discussed in Baradaran Shoraka et al. [25]. These mechanisms can be categorised in to three groups:

  i.   Side-sway collapse

This mechanism may be obtained from incremental dynamic analysis (IDA) and it corresponds to the system experiencing large increase of lateral deformations with small increase in seismic intensity. This mechanism is usually observed with ductile-structures that consist of components which are capable of experiencing large deformations prior to axial load failure.

  ii.   First component failure

Collapse of a building is determined based on the first component within the building to reach the collapse limit state. This is the approach which is usually adopted by codes, including ASCE/SEI 41 [18].

  iii. Gravity-load collapse (system collapse)

Collapse of a building is dependent on multiple components reaching the collapse limit state which will cause a global or system collapse of the building. Baradaran Shoraka et al. [25] define gravity collapse as when the gravity load demand exceeds the gravity load capacity for a particular storey for the assessment of RC frames. It is noted this mechanism of collapse limit can only be conducted if the nonlinear model has the ability to accurately simulate shear strength and axial load capacity degradation.

In this study, the Complete damage (*Collapse Prevention*) limit state is defined as when the first component reaches axial load failure. Hence the first component failure mechanism for defining a performance limit is adopted which is consistent with the approach adopted for all the other performance limits. The system collapse mechanism is not adopted because: (i) the degradation of axial load capacity is not modelled due computational efficiency and numerical stability, (ii) accurate models (which are usually empirically based) for simulating axial load failure are limited and further research is required in this area, and (iii) the loss of axial load failure in one component is likely to be followed immediately by other components.

In this study the Complete damage performance limit state is based on the axial failure limit reached by the perimeter frame components. This is defined as the

rotation corresponding to a 50 % reduction of the ultimate moment capacity Figure 1. This limit has been defined (instead of the calculated rotation at axial load failure for columns/beams, and the rotation corresponding to residual strength for joints) to provide some conservatism in defining the axial load failure due to the limitations of the model. This includes the limited availability of experimental results to define and to validate axial load failure deformation limits for components. It is also noted that in this study, it is assumed that the frame elements will undergo axial load failure prior to the primary lateral load resisting system. This is because the walls have relatively low axial load and it is expected that they will continue carrying the limited axial load after their ultimate lateral strength capacity is reached. Furthermore, drifts are limited to 2.0 % to provide a precaution to side-sway collapse mechanism.

Summary of performance levels

A summary of the adopted performance levels is provided in Table 1. The structural damage limits defining performance levels based on component responses are illustrated graphically in Figure 1.

(a) For RC wall buildings

Performance limit	Primary structure
Slight Damage / Serviceability (S)	Wall reaching a compressive strain of 0.001, or tensile strain of 0.005, whichever occurs first
Slight Damage/ Damage Control (DC)	Wall reaching a compressive strain of 0.002, or tensile strain of 0.01, whichever occurs first
Moderate Damage/ Life Safety (LS)	Wall reaching ultimate rotational limit, corresponding to a compressive strain of 0.003, or tensile strain of $0.6\varepsilon_{su}$, whichever occurs first
Extensive Damage/ Collapse Prevention (CP)	NA

(b) For RC frames building

Performance limit	Primary structure	Secondary structure	Non-structural limit
Slight Damage / Serviceability (S)	Wall reaching initial yield limit	Frame component reaching nominal yield rotational limit	0.004
Slight Damage/ Damage Control (DC)	Wall reaching a compressive strain of 0.002, or tensile strain of 0.015, whichever occurs first	Frame component reaching rotation which is at mid-point between yield and ultimate rotational limits	0.008

Moderate Damage/ Life Safety (LS)	Wall reaching ultimate rotational limit, corresponding to a compressive strain of 0.004, or tensile strain of $0.6\varepsilon_{su}$, whichever occurs first	Frame component reaches the rotation corresponding to shear failure	0.015
Extensive Damage/ Collapse Prevention (CP)	NA	Frame component reaches the rotation corresponding to 50 % reduction in ultimate lateral strength	0.002

NA: Not applicable

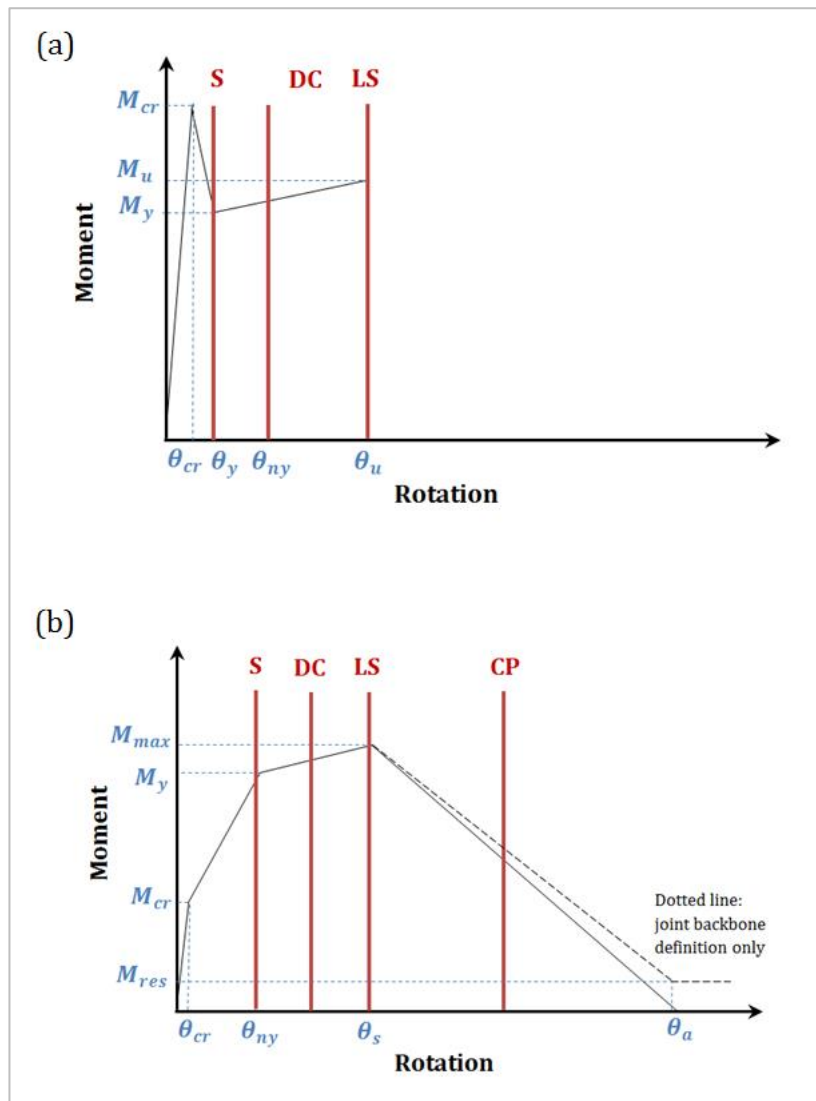TABLE 1: SUMMARY OF THE ADOPTED PERFORMANCE LEVELS

FIGURE 1 GRAPHICAL REPRESENTATION OF PERFORMANCE LIMITS, (A) WALLS, (B) FRAME COMPONENTS

GROUND MOTION INTENSITY MEASURE

The development of fragility curves involves conditioning the structural response on the ground motion intensity measure (IM). It is critical that the IM selected shows a strong correlation between the seismic intensity and the structural response to reduce the uncertainty in the seismic assessment. In addition, the IM

needs to effectively represent the level of seismic hazard, that is, it needs to be a parameter that can be correlated to various earthquake return periods [26].

Many different IMs exist and the choice of a suitable parameter is highly dependent on the type of analysis conducted and the type of structure which is being assessed. The IMs may be classified broadly in to two categories; structure-independent and structure-specific IM [4]. Structure-independent IM include parameters which define the ground motion properties, including: peak ground acceleration (PGA), peak ground velocity (PGV), peak ground displacement (PGD) and duration of the earthquake. Structure-specific IM include spectral response parameters calculated at a specific period and therefore they account for the frequency content of the ground motion and the fundamental or effective building period of vibration. A third category may also be considered which includes the maximum spectral response parameters; maximum spectral acceleration response ($\mathrm{RSA_{max}}$), maximum spectral velocity response ($\mathrm{RSV_{max}}$) and maximum spectral displacement response ($\mathrm{RSD_{max}}$). While the parameters are independent of the fundamental building period, their suitability may be dependent on the general fundamental period of the buildings assessed. For example, $\mathrm{RSD_{max}}$ is typically suitable for predicting the response of long-period structures whereas $\mathrm{RSA_{max}}$ is suitable for short period structures.

Traditionally, the IM that has been commonly used for seismic assessment has been PGA. It is the parameter which is typically used to represent hazard on seismic hazard maps, including AS 1170.4:2007. However, the seismic hazard factor (Z) in AS 1170.4 is a nominal value and it is calculated by dividing the PGV values (in millimetres per second) by 750 [27]. This is because PGV is considered to provide a better indication of the level of structural damage since it is related to the energy in the ground motion [27,28].

More recently, the use of structure-specific IMs have been used for for conducting assessment. This category of IM has the ability to relate the seismic demand to the structural properties of the buildings assessed. The most commonly used IM is the pseudo-spectral acceleration, typically calculated at the fundamental building period ($\mathrm{RSA(T_1)}$) [27]. While it has been shown that $\mathrm{RSA(T_1)}$ is a more efficient parameter than PGA to determine structural damage it typically provides a poor indication of structural damage for buildings with higher fundamental periods or for buildings located on soil sites. Numerous studies have shown that the spectral displacement response provide a better indication of structural damage. Interestingly, while the spectral displacement response has been widely used to conduct non-linear static assessment, it is typically not selected as an IM for the development of fragility curves from dynamic time-history analyses. This may be due to the fact that hazard studies and maps typically correlate with PGA, PGV and RSA(T) to earthquake return period events.

GROUND MOTIONS FOR TIME-HISTORY ANALYSIS

One of the main challenges of conducting assessment of buildings in low-to-moderate seismic regions is the selection of ground motions. In this study unscaled records have been selected such that they cover a wide range of IM values and are characteristic of Australian earthquakes. The records selected are a combination of: (i) stochastically generated records obtained using the program GENQKE [29] which is capable of producing ground motions that are representative of Australian earthquakes, (ii) historical records with characteristics representative of Australian earthquakes, including that they are shallow earthquakes with reverse fault mechanisms [30], (iii) simulated records on soil conditions by using equivalent linear [31] and non-linear site response program DEEPSOIL [32], using generated and historical rock records as input ground motions. It is noted that DEEPSOIL; which is capable of conducting nonlinear analysis was used for the input records that may have caused the soil strain to exceed the limits for which equivalent linear analyses are valid. The soil profiles used are presented in Figure 2.
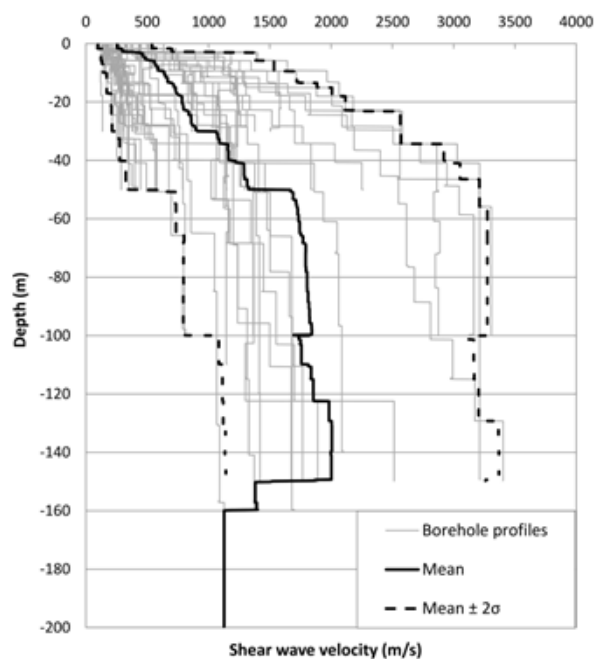

FIGURE 2 SHEAR WAVE VELOCITY PROFILES OF 50 SITES AROUND AUSTRALIA FROM KAYEN ET AL. [33]

//

ARCHETYPE BUILDING CHARACTERISTICS AND NONLINEAR MODEL

The following subsections describe the archetype RC building characteristics, including building design and detailing, the material properties adopted for assessment, and the nonlinear model created for time history analyses.

MATERIAL PROPERTIES FOR ASSESSMENT

When assessing the performance of existing structures it is ideal to use material properties obtained from the structures which are being examined. This is because there are many different factors that can cause a difference in material properties (especially strength) from the specified design values. However, when assessing the performance of a class of buildings using the approach of developing archetype buildings it is necessary to use probable or expected material properties. These values are usually based on testing conducted on a large number of samples taken from existing structures or from products produced by manufacturers. The median or mean values are adopted in this study, since studies which have investigated the effect of using random combination of material strengths using sampling methods (such as Latin Hypercube Sampling) have concluded that the effect is negligible in comparison to using mean/median material properties [5, 34].

The following subsections discuss the probable material properties adopted in this study to assess the performance of the archetype buildings.

Concrete

The average concrete compressive strength can vary significantly from the specified characteristic design strength for numerous reasons, including: the target strength (average value) being higher than the characteristic value used in design which is a 5 percentile value; quality of construction (noting that quality control may have been less stringent with older buildings); and concrete aging. Therefore, it is difficult to predict the probable strength of concrete without in-situ testing from the structures to be assessed.

The collapse of the Pyne Gould building and failure of the RC wall in the Gallery Apartments building after the Christchurch earthquake were discussed. In the case of the Pyne Gould building, concrete strengths of some concrete structural elements were reportedly much higher than the specified characteristic compressive strength (f'_c), corresponding to increased strength factors (K), calculated using equation 2.26, of 2.0 and 2.4 for the columns and beams respectively [35]. Similar concrete testing by Holmes Solutions [36] of the failed RC wall in the Gallery Apartments building indicated a κ value of up to 1.9. Data presented by [37] for strength gain with time of concrete made with different portland cements shows the relative mean strength with time, thus "relative [mean] strength" of concrete varying between 1.1 and 1.7. These values are likely to be higher if the strength gain with time was given relative to the f'_c.

Cook et al. [38] discuss proposed changes to the New Zealand Concrete Structures Standard, NZS 3101, which suggested that the concrete compressive strength is multiplied by a factor of 1.2 to convert from the lower characteristic

concrete compressive strength (f_c') to the average target compressive strength, and by 1.1 to increase the concrete compressive strength due to age. The technical guideline for seismic assessment of existing building provided by NZSEE [39] recommends taking the probable compressive strength of concrete as 1.5 times the characteristic concrete compressive strength. This factor specifically accounts for the increase in compressive strength of concrete due to age and the ratio between probable and lower characteristic strength (i.e. fifth-percentile) values. The factor for aging is predominantly based on the recommended equation by Eurocode 2 Part 1 [40] where the aging factor asymptotes after 10-20 years to approximately 1.2 to 1.4 depending on the cement class.

Recently, a study was conducted by Foster et al. [41] which focused on the statistical analysis of material properties in an Australian context. It is discussed that the compressive strength of concrete in a finished structure (f_c) can be taken as:

$$f_c = K_c K_w f_{cyl}'$$ (8)

Where K_c is a factor to account for the curing procedure

               K_w is a factor to account for workmanship

Foster et al. [41] suggest using the statistical data provided by Pham [42] to calculate the compressive strength of concrete in a finished structure. Based on more than 200 tests collected between 1962 and 1981, Pham reported the mean ratio of the 28 day concrete cylinder strength (f_{cyl}') to the specified concrete compressive strength (i.e. the characteristic concrete compressive strength, f_c') to be 1.18, and the mean factor accounting for curing process and workmanship to be 0.88. Therefore, the mean ratio of the compressive strength of concrete in a finished structure to the specified concrete compressive strength is 1.03 (i.e. $mean\ (f_c/f_c') = 1.03$).

Due to the uncertainty of predicting the probable compressive strength of concrete, a lower bound estimate is usually preferred. However, this may not always result in conservative estimates, especially when determining the failure mechanism of lightly reinforced walls. This is because a lower estimate of the compressive concrete strength may lead to a lower estimate of the tensile strength of concrete. Furthermore, it is also critical to account for the fact that the compressive strength of concrete in structures is highly dependent on the curing process and workmanship as considered in Pham [42] and Foster et al. [41].

For the RC shear wall buildings, the probably compressive strength is conservatively adopted as 1.5 times the characteristic concrete compressive strength (f_c') based on recommendation by NZSEE [39]. For the RC frames buildings the probable concrete compressive strength is taken as 1.2 times the characteristic concrete compressive strength (f_c') based on recommendations by Pham [42]. This accounts for the mean relationship between that the

compressive strength of concrete in a finished structure and the specified concrete compressive strength, as suggested by Pham [42] (i.e. $mean\,(f_c/f_c') = 1.03$) and an aging factor of approximately 1.2.

The tensile strength of concrete is usually conservatively ignored in the design and assessment of RC beams and columns. However, it is necessary to consider the tensile strength of concrete when assessing the performance of RC walls as, if it is neglected it may lead to non-conservative or overly conservative results depending on the failure mechanism of the wall. If the tensile strength of concrete is not considered or it is under-estimated then the mechanism which leads to single crack or minimal cracking of lightly reinforced walls may not be detected. Hence, care should be taken when determining the failure mechanisms of components and the effect of the assumption of material properties.

The tensile strength of concrete is often represented in two forms: (i) uniaxial tensile strength of concrete (f_{ct}), and (ii) flexural tensile strength ($f_{ct.f}$). The Australian Standard, AS 3600:2009, recommends in the absence of accurate data that the mean uniaxial tensile strength of concrete and the mean flexural strength of concrete according to Eq. (9) and Eq. (10), respectively.

$$mean(f_{ct}) = 1.4 \times 0.36\sqrt{f_c'} = 0.50\sqrt{f_c'} \qquad (9)$$

$$mean(f_{ct.f}) = 1.4 \times 0.6\sqrt{f_c'} = 0.84\sqrt{f_c'} \qquad (10)$$

For the purpose of assessment, Cook et al. [38] propose calculating the tensile strength of concrete using Eq. 11 for flexural cracking. The 1.2 factor is included to account for the gain in tensile strength due to age.

$$assessment(f_{ct.f}) = 0.55\sqrt{1.2f_c'} \approx 0.60\sqrt{f_c'} \qquad (11)$$

The model code proposed by the International Federation for Structural Concrete [43], assumes that the flexural tensile strength of concrete is a function of the uniaxial strength of the concrete and the depth of the RC member. It is suggested that the mean flexural tensile strength of concrete be calculated in accordance with Eq. (12). The equation accounts for the fact that the flexural tensile strength is approximately equal to the axial tensile strength of concrete for members with deep sections.

$$mean(f_{ct.f}) = \frac{mean(f_{ct})}{A_{fl}} \qquad (12)$$

Where $mean(f_{ct})$ is the mean uniaxial tensile strength

A_{fl} is a factor which account for the depth of the component:

$$A_{fl} = \frac{0.06h^{0.7}}{1+0.06h^{0.7}}$$

where h is the depth of the member (i.e. wall length for walls and cores)

In this study, the equation proposed by Cook et al. [38] is adopted for RC walls and RC frames buildings since it has been specifically derived for the purpose of assessment.

Steel reinforcement

RC shear wall buildings

D500N reinforcing bars are used in the assessment of RC shear wall buildings. It is estimated that over 60% of all Class N type reinforcing bars in Australian building construction are either 12 or 16 mm in diameter, most of which are used in either RC slabs or walls as the main flexural reinforcement. The mechanical properties of the bars have been adopted from test results by Menegon [44] and are presented in Table 2. These values can be compared to the lower characteristic values given in AS/NZS 4671:2001 [25] (presented in Table 3).

	f_Y (MPa)	f_u (MPa)	f_u / f_Y	ε_{sh}	ε_{su}
Mean	551	660.5	1.201	0.0197	0.095
Standard Deviation	29.2	37.7	0.076	0.0095	0.029

TABLE 2: MEAN AND STANDARD DEVIATION VALUES OF D500N REINFORCEMENT FROM (MENEGON, 2015)

	f_Y (MPa)	f_u (MPa)	f_u / f_Y	ε_{su}
D500N	500	515	1.03	0.015

TABLE 3: LOWER CHARACTERISTIC VALUES OF REINFORCING BARS FROM AS/NZS 4671:2001

The values of material properties are selected at random from a generated number based on a normal distribution or are randomly chosen between an appropriate minimum and maximum range. For example, the yield and ultimate stress of the reinforcing steel (f_Y and f_u) are calculated from a random number using a normal distribution with a mean (μ) and standard deviation (σ) taken from the results reported in Menegon *et al*. [44] for D500N reinforcing steel.

RC frames buildings

The idealised buildings assessed are representative of buildings constructed in the late 1980s and therefore they are likely to have 410Y or 400Y bars as the main reinforcement. There were two types of Y-bars which were available in Australia: *Tempcore*, supplied by BHP and *Welbend*, supplied by Smorgon Steel. The tensile steel properties provided in the *Tempcore* and *Welbend* specifications document are summarised in Table 4. In addition, the nominal properties specified by AS 1302 [46] are also provided in Table 5 for comparison. It is noted that both suppliers report the total elongation strain rather than the uniform elongation strain (i.e. the ultimate strain) and thus the uniform elongation strain values provided in Table 4 are obtained from the typical stress-strain curves provided in the specifications handbook (provided in Figure 3) for the purpose of comparison. The total and uniform elongation values are defined as shown in Figure 3(b).

Based on the material properties presented in Table 4, it can be seen that the *Welbend* Y-bars tend to have better tensile properties than the *Tempcore* Y-bars. Hence the mean material properties of *Tempcore* Y-bars are adopted in this study to avoid over-prediction of the reinforcement properties.

	f_y (MPa)	f_u / f_y	Uniform elongation ε_{su}	Total elongation
AS 1302: nominal values	400-410	1.05-1.1	0.12-0.16	NA
Tempcore: mean properties	460	1.21	0.12[*]	0.25
Tempcore: standard deviation	17	0.03	NA	0.02
Welbend: mean properties	495	1.26	0.21[*]	0.268
Welbend: standard deviation	20.6	0.035	NA	0.017

[*]Uniform elongation values based on testing have not been reported, the values presented in this table are obtained from typical stress-strain curves provided in the specifications by the suppliers

TABLE 4: MEAN AND STANDARD DEVIATION VALUES OF Y-BARS

	f_y (MPa)	f_u / f_y	Uniform elongation ε_{su}	Total elongation
AS 1302: nominal values	400-410	1.05-1.1	0.12-0.16	NA

TABLE 5: NOMINAL VALUES OF REINFORCING BARS FROM AS1302:1991
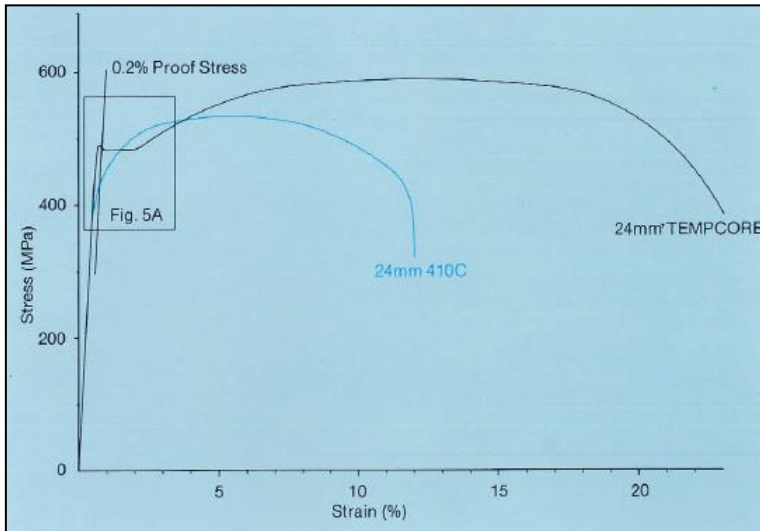
(a)
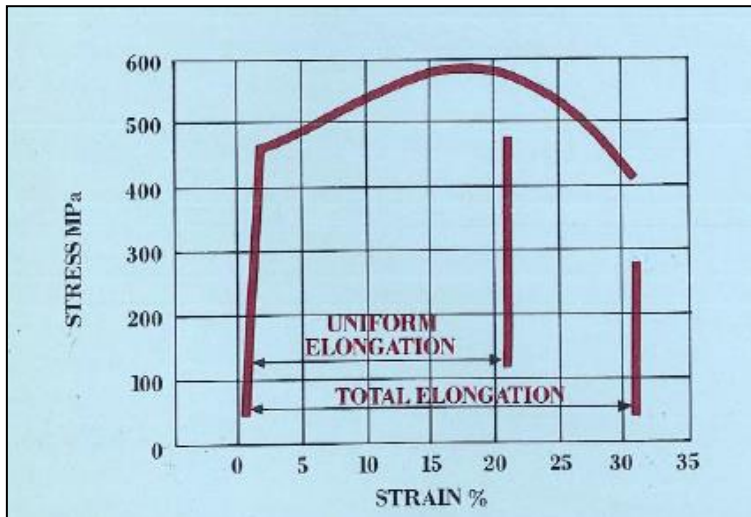
(b)

FIGURE 3: TYPICAL STRESS-STRAIN CURVES FOR Y-BARS PROVIDED BY: (A) TEMPCORE, (B) WELBEND

BUILDING DESIGNS

The following sections present the configuration of buildings and design of structural elements adopted in this study.

RC wall buildings

Four archetype buildings, varying by the use of rectangular and/or C-shaped RC walls for the lateral load resisting elements, are used in representing the idealised buildings for Australia. Four building configurations will be used; Type 1, Type 2, Type 3 and Type 4, which are illustrated in Figure 4. Only particular building types can be used to represent the Low-Rise, Mid-Rise and High-Rise structures, which is dependent on the number of storeys; this is because the buildings will be initially designed for earthquake loading (using AS 1170.4:2007) and/or wind loading (using AS 1170.2:2011). For example, a High-Rise building may not have the (moment) capacity for the earthquake or wind demand if it only has C-shaped centralised walls (building Type 3). Therefore, HR buildings are limited to Type 4. Moreover, the single C-shaped wall building (Type 2) is limited to LR buildings designed pre-1995, before earthquake loading became a design requirement. It should be noted that it is assumed for all buildings that center of stiffness provided by the lateral load resisting walls for each principle direction is close to the center of mass; therefore, the effects of torsional displacement due to in-plane asymmetry have been neglected in this study. It should also be emphasised that the HR buildings investigated here have a 12-storey limit. A large percentage of the RC walls laterally supporting LR buildings would result in a low aspect ratio (A_r). The RC walls that have been studied have been governed primarily by flexure and have had an A_r higher than 2. Furthermore, for this study the C-shaped walls are assumed to be uncoupled. This assumption is only valid for moderate "High-Rise" structures, since a coupled and stiffer centralised core (boxed section) would be typical for very tall structures.
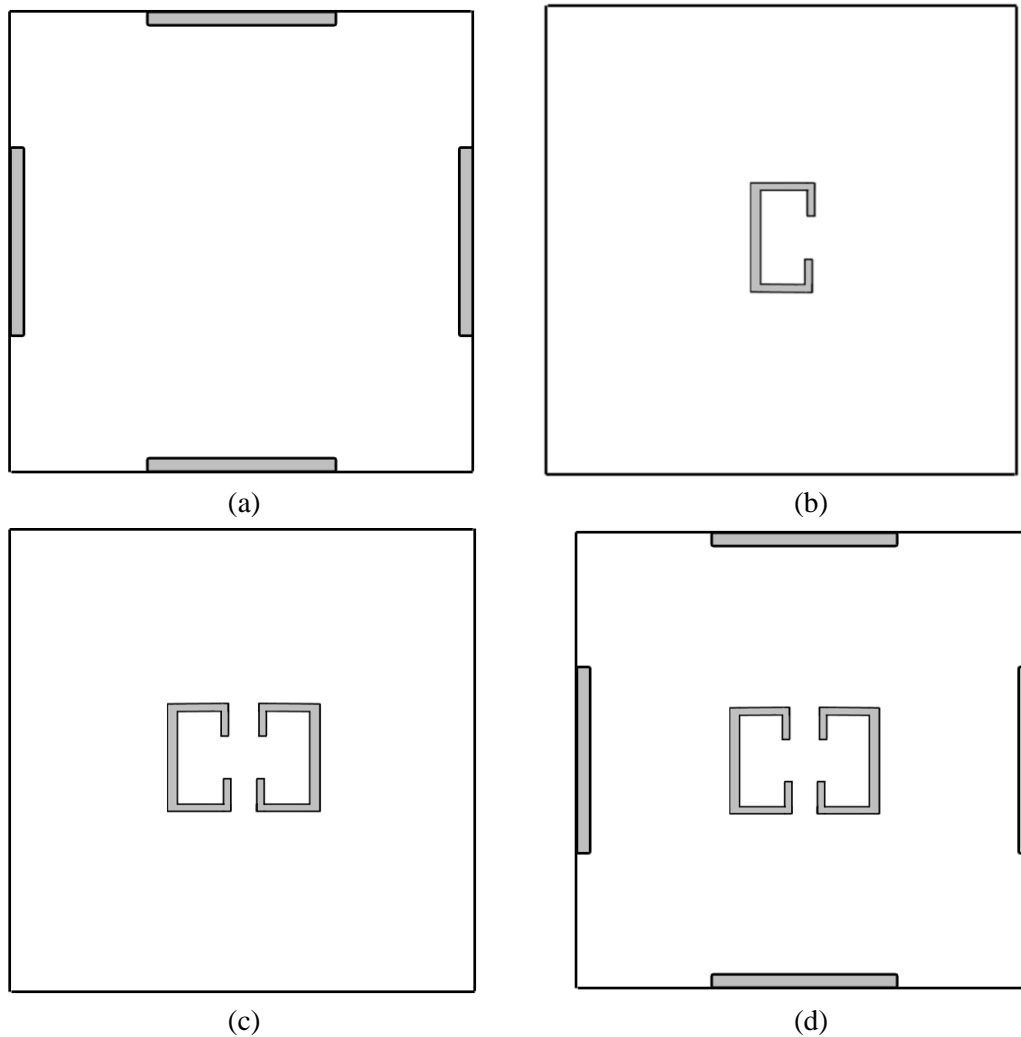
FIGURE 4: THE DIFFERENT IDEALISED BUILDING CONFIGURATIONS USED FOR RC BUILDINGS IN AUSTRALIA (A) TYPE 1 (B) TYPE 2 (C) TYPE 3 AND (D) TYPE 4

Table 6 presents the different Building Types and limiting number of storeys (n). The definition of the Low-Rise, Mid-Rise and High-Rise corresponds to the number of storeys has been adopted from (FEMA, 2010). This definition has also been adopted in Geoscience Australia's Earthquake Risk Model (EQRM) [48] and GAR15 [49].

Building Type	minimum n	maximum n	Rise
1	2	4	Low, Mid
2	2	3	Low
3	2	7	Low, Mid
4	4	12	Mid, High

TABLE 6: BUILDING TYPES WITH LIMITING NUMBER OF STOREYS (N)

The range of values used for some of the building parameters are summarised in Table 7. In contrast to the values for some parameters selected on the basis of a normal distribution, the axial load ratio (*ALR*), for example, is randomly chosen between a minimum of 0.01 (1%) and a maximum of 0.1 (10%), based on common values used in previous research [50] as well as investigations by Albidah *et al.* [51] for low-to-moderate seismic regions and more recently Menegon *et al.* [52] for Australia. Other parameters given in Table 7 that are

varied within the maximum and minimum values include the dead and live load of the building per floor (G and Q respectively), inter-storey height (h_s), longitudinal reinforcement ratio (ρ_{wv}). The length of the rectangular walls (L_w) are chosen randomly between a value of 0.17B and 0.33B, where the width of the building (B). The dimensions of the C-shaped walls for Building Types 2, 3 and 4 in Figure 4 are based on the number of storeys; the different Building Types and range of allowable storeys (n) are presented in Table 8.

Parameter	μ	σ	min	max	constant	Units
ALR	-	-	0.01	0.1[a]/0.05[b]		-
G	-	-	4	8		kPa
Q	-	-	1	4		kPa
h_s	-	-	3.0	3.5		M
ρ_{wv}	-	-	0.19%	1.00%		-

a = Rectangular walls
b = C-shaped Walls

TABLE 7: WALL PARAMETERS AND VALUES CONSIDERED FOR THE VULNERABILITY ASSESSMENT PROGRAM

Wall	t_w (mm)	L_{web} (mm)	L_{flange} (mm)	L_{return} (mm)
LR	200	3600	2000	600
MR	200	6200	2200	600
HR	250	8500	2500	600

TABLE 8: DIMENSIONS OF THE C-SHAPED WALLS

RC frames buildings

Six archetype buildings are assessed which are 2-, 5-, and 9-storey high. The buildings are representative of older RC buildings constructed in Australia prior to the requirement for seismic load and design to be mandated on a national basis. The buildings have been designed in accordance with AS 3600:1988 Concrete Structures Standard, AS 1170.2:1983 Wind Actions Standard, and guidance from experienced practicing structural engineers. The frames are designed as ordinary moment resisting frames (OMRFs). The core walls have low longitudinal reinforcement ratio (approximately 0.23 %) with no confinement and thus are likely to develop a single crack under lateral loading. The building plans are provided in Figure 5. The gravity load resisting system of the buildings constructed in the 1980s typically included perimeter frames with deep beams (600-900 mm deep) to satisfy fire design requirements, and band-beams or flat-slab floor systems with column spacing of 7.0 to 8.4 m. Hence for the archetype buildings the typical column spacing of 8.4 m is adopted with perimeter beam depth of 650 mm. The design properties of the building components are provided in Table 9, and the detailing of the frame components and the core walls are provided in Figures 6 and 7, respectively. Details of the interior system are not provided as the interior gravity system is not modelled since it is expected that the perimeter frames will fail prior to the interior gravity system. This is because the perimeter frames have significantly higher stiffness in comparison to the interior gravity frames and therefore they will be subjected to greater seismic forces in comparison to the interior gravity system.
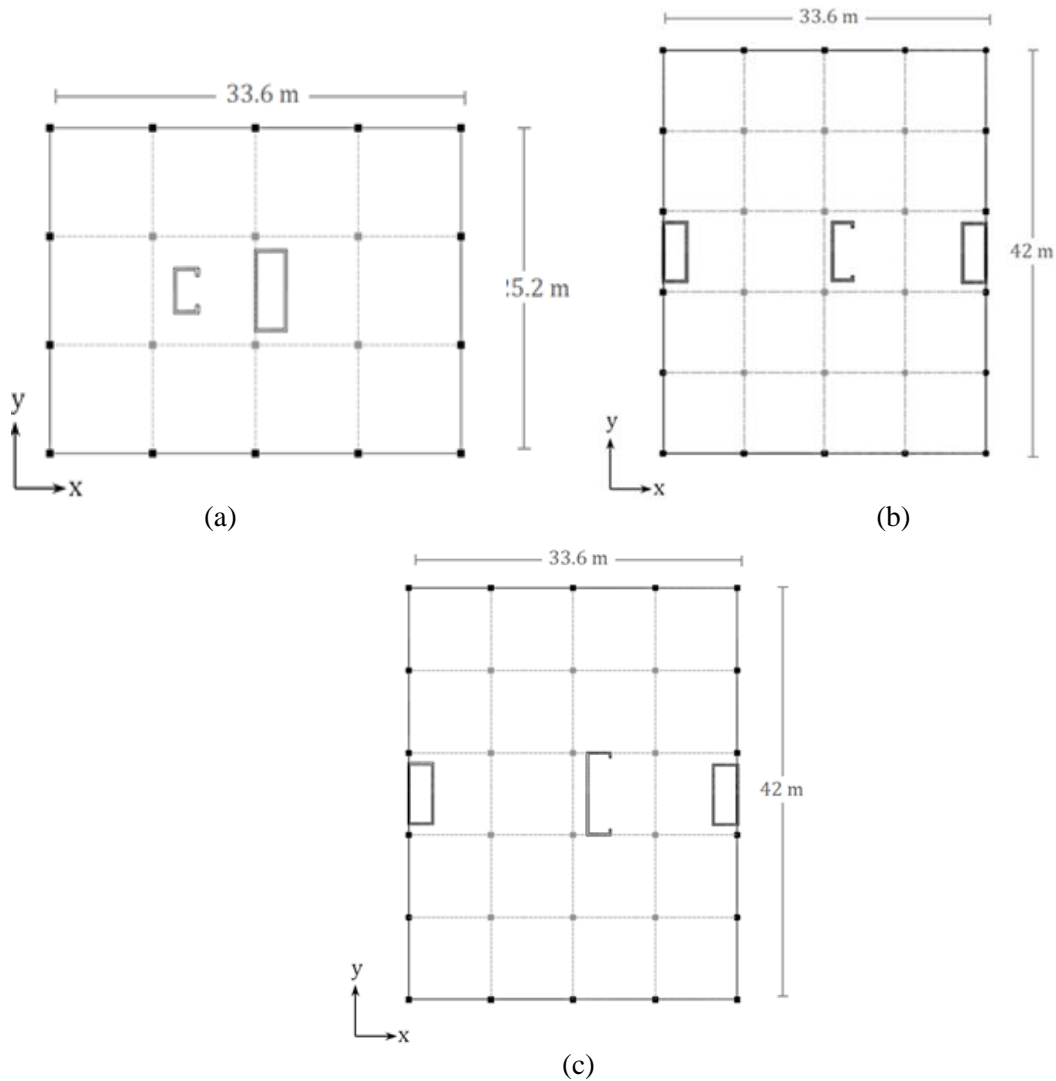
(a)

(b)

(c)

FIGURE 5: BUILDING PLANS OF ARCHETYPE BUILDINGS, (A) 2-STOREY, (B) 5-STOREY AND (C) 9-STOREY

	Slab	Perimeter beams	Columns	Core walls
f'_c (MPa)	25	25	40	40
f_y (MPa)	400	400	400	400
ρ_l (%)	0.67-1.33	1.30-2.70	2.0-4.0	0.23-0.24
ρ_t (%)	0.25	0.23	0.075-0.12	0.25

f'_c: characteristic concrete compressive strength | f_y : nominal reinforcement yield strength | ρ_l: longitudinal reinforcement ratio | ρ_t: transverse reinforcement ratio

TABLE 9: SUMMARY OF DESIGN PROPERTIES FOR BUILDING COMPONENTS

Typical beam design (near supports)*	Typical column design

2-storey building
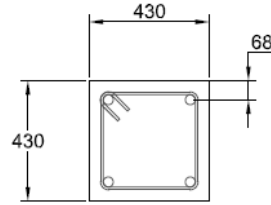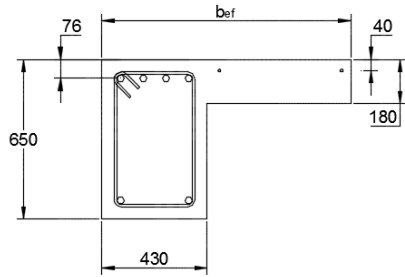
5-storey building
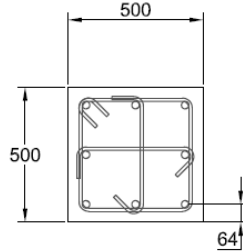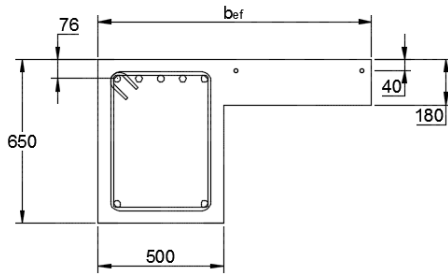
9-storey building
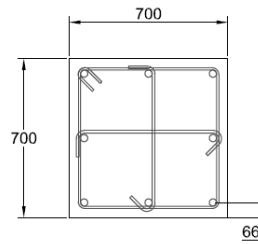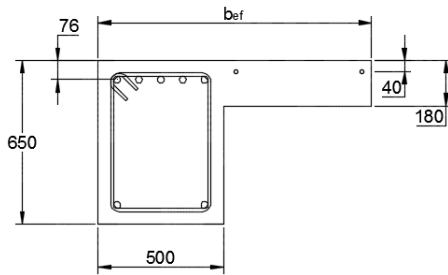
* Effective width of flange (b_{ef}) is also illustrated and it is calculated in accordance with AS 3600:2009.

FIGURE 6: PERIMETER BEAM AND COLUMN DESIGNS FOR ARCHETYPE BUILDING

Typical lift core design (similar for all storeys)

2-storey building lift core design
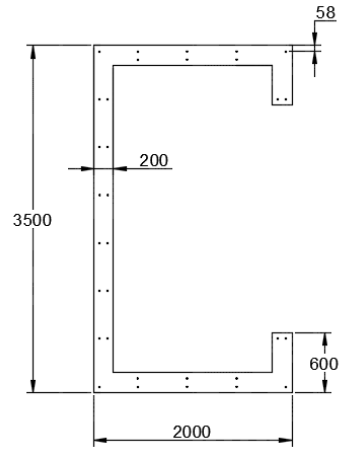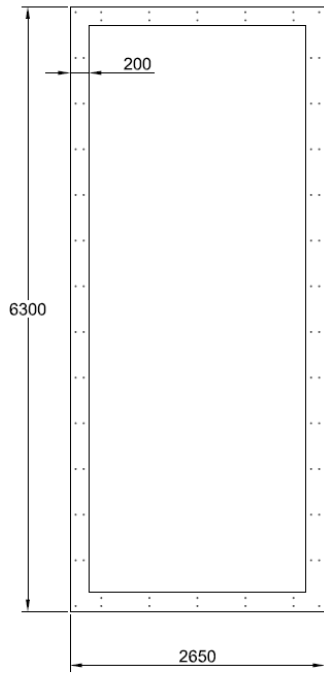
5-storey building lift core design

9-storey building lift core design
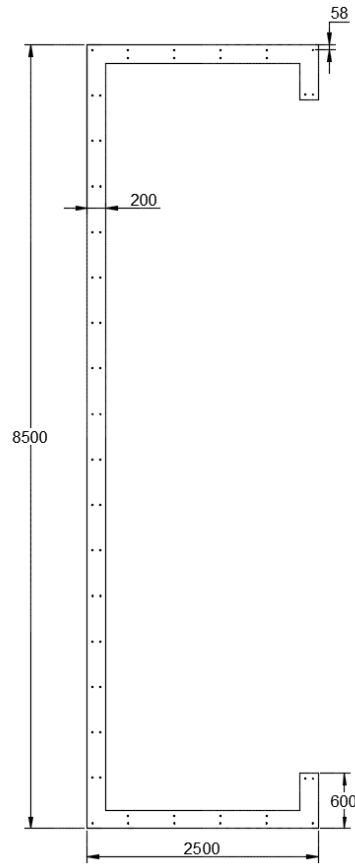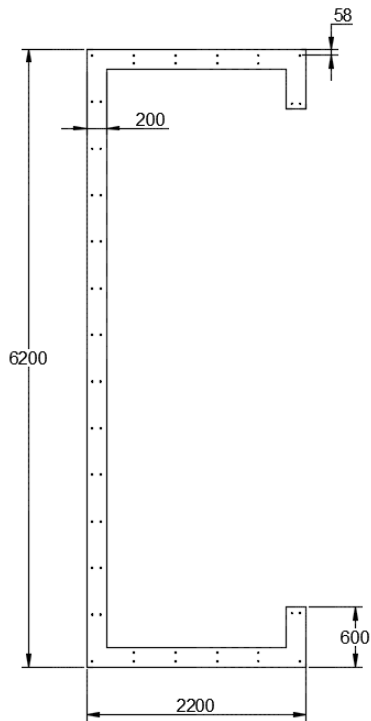
FIGURE 7: STAIR AND LIFT CORE DESIGNS FOR ARCHETYPE BUILDINGS

NON-LINEAR ANALYSES

The following sub-sections presents the modelling and analysis approach adopted to construct fragility curves of limited ductile reinforced concrete buildings.

RC wall buildings

A large number of analyses are to be undertaken using the capacity spectrum method CSM (in MATLAB) in order to obtain the fragility functions for RC shear wall buildings in Australia. In this sub-section, the CSM to obtain the fragility functions are validated by comparison with non-linear dynamic time history analysis NDTHA. Two different building configurations are used for four different case studies; a Mid-Rise (MR) building with rectangular (peripheral) walls and a MR building with central C-shaped cores. The two different building types are illustrated in Figure 8.
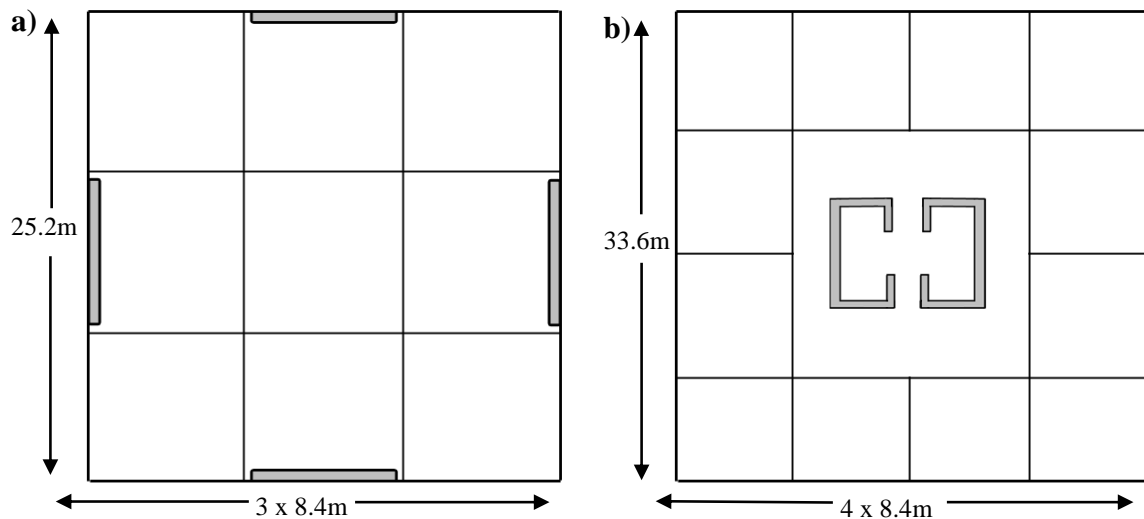

FIGURE 8: PLAN VIEW OF MID-RISE BUILDING WITH (A) PERIPHERAL WALLS AND (B) C-SHAPED CORES

For each building type (shown in Figure 8), two different longitudinal reinforcement ratios (ρ_{wv}) have been used in the RC walls (Table 10). Based on studies by Hoult et al. [53], for each building type, a single primary crack is expected to form on the walls with lower longitudinal reinforcement whilst secondary cracks will form on the walls with higher longitudinal reinforcement. The assumed value of the in-situ concrete strength (f_{cmi}) is 40 MPa for the RC walls. Other building parameters, such as dead load (G), live load (Q), inter-storey height (h_s), number of storeys (n) and breadth and depth of the building (B and D) are given in Table 11. The values used for the parameters represent typical values found in the Australia and other low-to-moderate seismic regions.

Building No.	Wall Type	ρ_{wv}	$\rho_{wv.min}$	L_w (mm)	t_w (mm)	L_f (mm)	L_r (mm)
1	R (Type 1)	0.70%	0.50%	7000	200	-	-
2	R (Type 1)	0.35%	0.50%	7000	200	-	-
3	C (Type 3)	1.00%	0.50%	6300	200	2650	600
4	C (Type 3)	0.40%	0.50%	6300	200	2650	600

TABLE 10: REINFORCEMENT RATIO AND DIMENSIONS OF THE RC WALLS

Building No.	Wall Type	G (kPa)	Q (kPa)	h_s (m)	B (m)	D (m)	n
1	R (Type 1)	4	1	3.5	25.2	25.2	5
2	R (Type 1)	4	1	3.5	25.2	25.2	5
3	C (Type 3)	6	2	3.2	33.6	33.6	5
4	C (Type 3)	6	2	3.2	33.6	33.6	5

TABLE 11: BUILDING LOADS AND DIMENSIONS

Capacity Spectrum Method CSM (in MatLab)

Building capacity

The building capacity, corresponding to the ultimate moment (M_U) of the walls (reflecting current design practice in Australia), is dependent on the building type and number of RC (rectangular and/or C-shaped) walls. Moment-curvature analyses (or "section analyses") will be used to calculate the capacities of the individual walls of each building. These values will also be used in some of the plastic hinge analysis expressions to obtain the force-displacement relationship of the RC walls. For the purposes of this study, the moment-curvature analysis program is incorporated within MATLAB to reduce computational time associated with using a third-program. Studies by Lam *et al*. [54] will be used as a guide to produce a moment-curvature (M-Φ) program in MATLAB. The stress-strain (σ-ε) relationship used for the concrete and reinforcing steel is calculated using expressions given in Wong *et al*. [55] for the Popovics (normal and high strength concrete) and Seckin [56] (back-bone curve) models respectively.

The MATLAB M-Φ program can be used to find the ultimate moment (M_U), as well as curvature and moments at different levels of strains that correspond to different performance levels. For the sake of brevity, the reader is referred to Lam *et al*. [54] for a full understanding of how the M-Φ program is created. The program was validated in Hoult (2017) by comparing the M-Φ output of many different walls and parameters to that obtained by third-part software. The ultimate moment capacity of the building (M_U) is determined from the contribution of all walls in the building for the given direction of loading. If ΦM_U is less than M^*, where Φ is taken as 0.8 from AS 3600:2009, then the process of calculating M_U is repeated using different generated values for the parameters of the walls (presented in Table 7). If the calculated ΦM_U of the building exceeds M^*, the program continues on to the next stage in calculating the displacement capacity and constructing the capacity diagram for the structure.

The displacement capacity of the walls are obtained Plastic Hinge Analysis (PHA). The PHA acknowledges that the top displacement of a cantilever wall structure is the summation of the deformation components primarily due to flexure, shear and slipping. These deformation components can be used to calculate the yield displacement (Δ_Y) and plastic displacement (Δ_P). The

calculations to determine the yield displacement (Δ_y), plastic displacement (Δ_p) and plastic hinge length (L_p) based on expressions derived by Hoult et al. (2017a; 2017b; 2017c). These expressions are summarised below, where the reader is referred to Hoult *et al.* (2017a), Hoult *et al.* (2017b) and Hoult *et al.* (2017c) for more information on their derivation.

$$\Delta_y = K_\Delta \Phi'_y (\frac{k_{cr}}{3} H_n^2 + L_{yp} H_n)(1 + \frac{\Delta_s}{\Delta_f}) \tag{13}$$

where k_{cr} is a factor derived by Beyer [57] and Constantin [58] to account for the actual height of the wall estimated to be cracked (Equation 16), Δ_s / Δ_f is the shear-to-flexure deformation ratio (Equation 17), L_{yp} is the yield strain penetration length (approximately 150 mm), Φ'_y is the curvature at first yield and K_Δ is a factor introduced by Hoult *et al.* [59] to account for lightly reinforced walls (Equation 14).

$$K_\Delta = \theta \rho_{wv} + \beta \tag{14}$$

where the θ and β parameters are given in Table 12.

C-Shaped			
	Rectangular	Major	Minor (WiC)	Minor (WiT)
θ	45	80	50	100
β	0.22	0.00	0.30	1.00

TABLE 12 PARAMETERS FOR THE K_Δ FACTOR

$$k_{cr} = \alpha + 0.5(1 - \alpha)(\frac{3H_{cr}}{H_n} - \frac{H_{cr}^2}{H_n^2}) \tag{15}$$

where α is the ratio of cracked to uncracked flexural wall stiffness ($E_c I_{cr} / E_c I_g$) and H_{cr} is the height of the cracked wall (Equation 16). It should be noted that the stiffness of the cracked section ($E_c I_{cr}$) can be estimated with M'_y / Φ'_y.

$$H_{cr} = \max\left(L_w, \left(1 - \frac{M_{cr}}{M'_y}\right)H_n\right) \tag{16}$$

where M_{cr} is the cracking moment and M'_y is the moment corresponding to first yield.

$$\frac{\Delta_s}{\Delta_f} = \begin{cases} 1.5\left(\frac{\varepsilon_m}{\Phi \tan\theta_c}\right)\left(\frac{1}{H_e}\right), & C-shaped\ walls \\ 0, & rectangular\ walls \end{cases} \tag{17}$$

where ε_m is the mean axial strain of the RC section (which can be estimated from a moment-curvature analysis), Φ is the curvature corresponding to a performance level and θ_c is the crack angle [with a recommended value of 30° [60] to be used for the assessment of existing structures].

$$\rho_{wv.min} = \frac{(t_w - n_t d_{bt})f_{ct.fl}}{f_u t_w} \tag{18}$$

where $\rho_{wv.min}$ is the minimum longitudinal reinforcement required to allow secondary cracking [61], t_w is the thickness of the wall, n_t is the number of grids

of horizontal (transverse) reinforcing bars, d_{bt} is the diameter of the horizontal reinforcing bars, $f_{ct.fl}$ is the mean flexural tensile strength of the concrete and f_u is the ultimate strength of the longitudinal reinforcing bars.

$$\Phi_{pl} = \begin{cases} \dfrac{0.6\varepsilon_{spl} - \varepsilon_{sy}}{L_w}, & \dfrac{\rho_{wv}}{\rho_{wv.min}} < 1 \\[2em] moment - curvature\ anlysis, & \dfrac{\rho_{wv}}{\rho_{wv.min}} \geq 1 \end{cases} \tag{19}$$

where Φ_{pl} is the curvature corresponding to a given performance level, ε_{spl} is the strain in the steel corresponding to a given performance level and L_w is the wall length.

$$L_p = \begin{cases} 150, & \dfrac{\rho_{wv}}{\rho_{wv.min}} < 1 \\[2em] (\alpha L_w + \gamma H_e)(1 - \delta ALR)(\omega e^{-\tau\nu}), & \dfrac{\rho_{wv}}{\rho_{wv.min}} \geq 1 \end{cases} \tag{20}$$

where H_e is the effective height, ALR is the axial load ratio, ν is the normalised shear parameter (Equation 21) and the five parameters in Equation 20 (α, γ, δ, ω and τ) are given in Table 13.

	A	γ	Δ	ω	T
Rectangular	0.1	0.075	6	1.0	0.0
C-shaped (Major)	0.1	-0.013	13	7.0	0.8
C-shaped (Minor, WiC)	0.5	-0.015	3	1.6	0.1
C-shaped (Minor, WiT)	1.0	-0.073	8	2.5	2.1

TABLE 13 PARAMETERS FOR L_P IN EQUATION **ERROR! REFERENCE SOURCE NOT FOUND.**

$$\nu = \frac{\tau}{0.17\sqrt{f_{cmi}}} \tag{21}$$

where τ is the average shear stress parameter, which can be calculated from a sectional analysis ("moment-curvature" analysis) or can be estimated by dividing the base shear (V_b) of the wall by the effective area (A_{eff}) of the section.

$$\Delta_p = L_p(\Phi_{pl} - \Phi'_y)H_e\left(1 + \frac{\Delta_s}{\Delta_f}\right) \tag{22}$$

$$\Delta_{cap} = \Delta_y + \Delta_p \tag{23}$$

The displacement capacity (Δ_{cap}) of a RC wall corresponding to different "performance levels" can thus be found.

Earthquake demand

Earthquake demands in the format of an acceleration-displacement response spectrum (ADRS) are used to evaluate the seismic performance using the capacity spectrum method. The displacement response (RSd) can be derived readily from the acceleration response (RSa) using Equation (24).

$$RSd = RSa \times \left(\frac{T}{2\pi}\right)^2 \tag{24}$$

For the purpose of the comparison with NDTH the buildings are assumed to be located in the Melbourne CBD. The earthquake spectra developed by Hoult [53] using Probabilistic Seismic Hazard Analysis (PSHA) have been adopted. The results from the PSHA study for Melbourne for a 500-year return period event was scaled such that the result is equal to a warranted intensity measure (IM); the IM used for the study in this section is the peak ground acceleration (PGA) parameter. Therefore, the 500-year return period acceleration response spectrum for Melbourne is scaled, starting from 0.05g and incremented by 0.05g up to 0.5g, and artificial ground motions are generated the scaled response spectra as target spectra. Six artificial acceleration-time histories were produced for each PGA increment from SeismoArtif [62] as illustrated in Figure 9. Moreover, if a single structure has not reached or exceeded a performance level (for all six ground motions), further analyses are required, and acceleration time-histories are created for 0.6g through to 1.0g (in increments of 0.1g). The artificial acceleration-time histories are used in the NDTHA to construct the fragility curves.

It should be noted that the method to derive earthquake demands described in this subsection is only used for the purpose of comparison between fragility curves constructed using CSM and NDTHA. For the construction of fragility curves of the RC buildings, the approach to obtain unscaled ground motions from historical and generated records described earlier has been used.
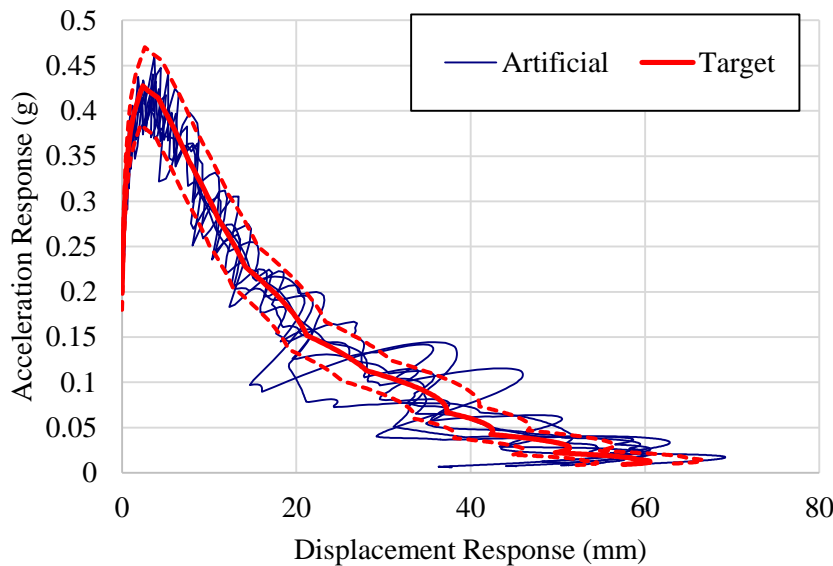

FIGURE 9 ACCELERATION-DISPLACEMENT DEMAND FOR PGA 0.2G

SeismoArtif uses a magnitude-distance (M-R) combination in an attempt to predict the ground motion at the site. The M-R combinations were selected for each different PGA increment based on the work from [63]. A maximum moment magnitude (Mw) of 7.5 was used for this study. The resulting M-R combinations used in SeismoArtif for the different PGAs are given in Table 14.

M	R (km)	PGA (g)
5.0	25	0.025

5.0	13	0.050
5.5	13	0.075
5.5	10	0.100
6.0	15	0.125
6.0	12	0.150
6.0	11	0.175
6.0	9	0.200
6.5	14	0.225
6.5	13	0.250
6.5	12	0.275
6.5	11	0.300
6.5	10	0.325
6.5	9	0.350
6.5	9	0.375
6.5	8	0.400
7.0	12	0.425
7.0	11	0.450
7.0	10	0.475
7.0	10	0.500
7.0	8	0.600
7.0	7	0.700
7.5	9	0.800
7.5	8	0.900
7.5	7	1.000

TABLE 14 M-R COMBINATIONS CALCULATED FOR THE DIFFERENT *PGA*S FOR MELBOURNE

The scaled target spectra (in the acceleration and displacement demand format) are used to construct fragility curves based on the Capacity Response Spectrum (CSM). CSM uses a relationship between the calculated displacement ductility (μ) and equivalent viscous damping (ξ_{eq}) to modify the elastic acceleration and displacement demand spectra. The damping is the sum of the elastic (ξ_{el}) and hysteretic (ξ_{hyst}) damping, given in Equation (25) from Priestley *et al*. [17] for RC cantilever wall structures.

$$\xi_{eq} = \xi_{el} + \xi_{hyst} = 0.05 + 0.444\left(\frac{\mu - 1}{\mu\pi}\right) \tag{25}$$

The ξ_{eq} is found for each of the corresponding displacements at the different performance levels. The spectral reduction factor (R_ξ) is then calculated using Equation (26), which has been adopted from the recommendations by Priestley *et al*. [17] without considerations of forward directivity velocity pulse characteristics.

$$R_\xi = \left(\frac{0.07}{0.02 + \xi_{eq}}\right)^{0.5} \tag{26}$$

The equivalent elastic spectral displacement capacity ($\Delta_{cap.el}$) for each of the performance levels is found using Equation (27).

$$\Delta_{cap,el} = \Delta_{cap}/R_\xi \tag{27}$$

Modelling approach for NDTHA

The two types of building configurations in Figure 8 were modelled in SeismoStruct. Force-based beam-column elements are used in SeismoStruct to represent the inelastic elements that will be used to construct the rectangular and C-shaped walls. Specifically, the inelastic plastic-hinge force-based frame elements (infrmFBPH) were used, which are considered to be elastic with a prescribed plastic hinge at the end node/s, as illustrated in Figure 10.

The infrmFBPH wall elements are made up of several different sections, the length of which is determined by the incrementing inter-storey height. The member section is divided into approximately 400 fibre sections. Different prescribed plastic hinge lengths were estimated for the infrmFBPH beam-column elements depending on the amount of the longitudinal reinforcement ratio used in the wall.
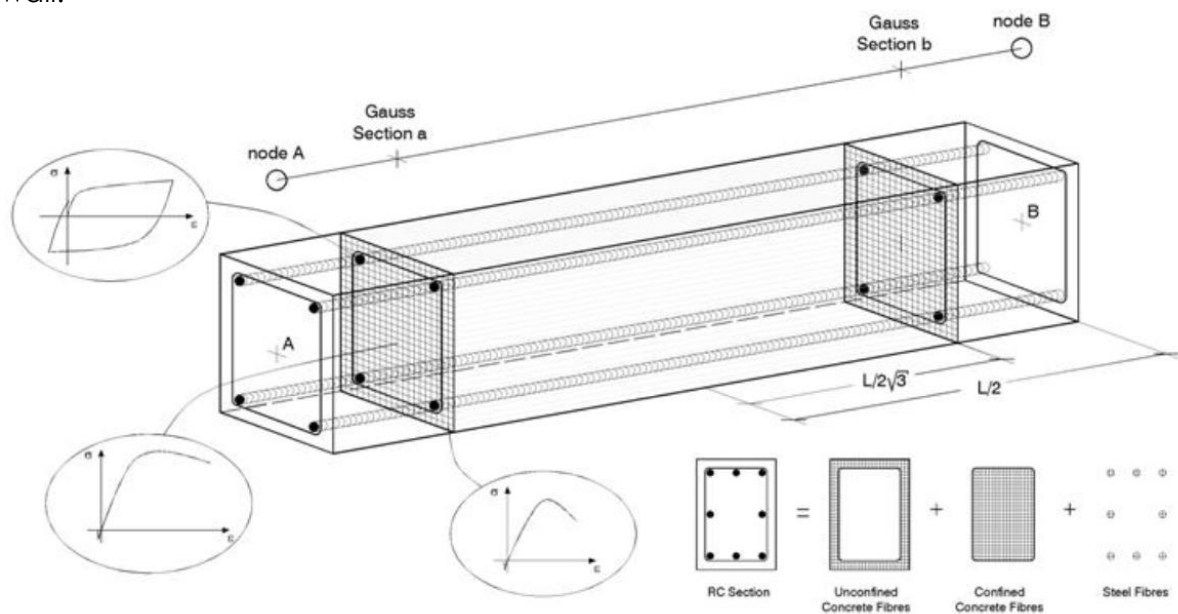
FIGURE 10: TYPICAL RC ELEMENT MODELLED IN SEISMOSTRUCT (SEISMOSOFT, 2013)

One rectangular RC section makes up the rectangular wall. Several rectangular sections make up the C-shaped wall: the web, flanges and returns. Using the "Wide-Column" analogy model, the rectangular sections of the C-shaped wall are connected using horizontal rigid links. This is illustrated in Figure 11, where the vertical elements (rectangular RC sections) of the web and flanges are connected by the horizontal links.
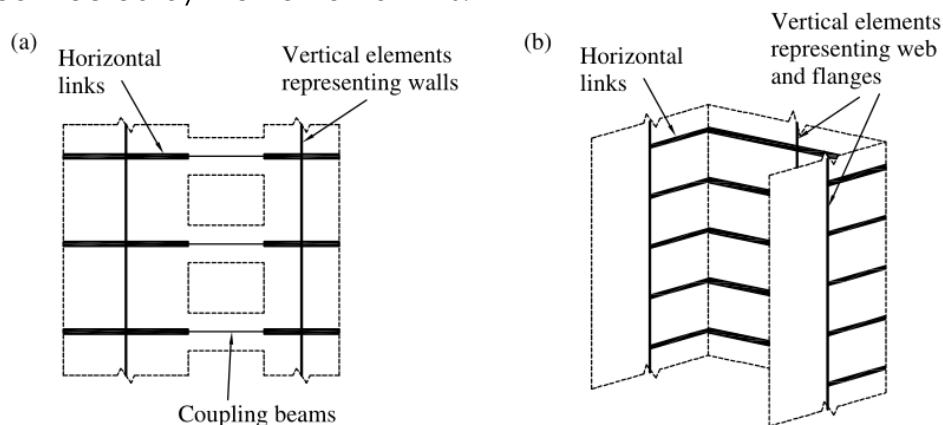
Figure 11: Wide column model of (a) a coupled wall system and (b) C-shaped wall from Beyer et al. [64]

Although SeismoStruct [65] offers a "U-shaped wall section" as a selectable section type, the wide-column model was chosen here to idealise the walls in order to include the contribution of the returns. Beyer et al. [64] has recommended that the spacing (vertically) of the horizontal links be based on one fifth of the shear span or half of the wall length. As half of the length of the web is approximately equal to the storey height (3100 mm compared to 3200 mm respectively), the rigid links were placed at the storey height for simplicity. A node was also placed at the effective height (H_e), in between two nodes at inter-storey height; this node was placed such that it would be possible to track the relative displacement at a height H_e from the node at the base of the wall. Rigid links were not applied for the nodes at H_e, as this would reduce the spacing size that was recommended. The rigid links, nodes and the different sections of the C-shaped wall used in the MR wall are illustrated in Figure 11.
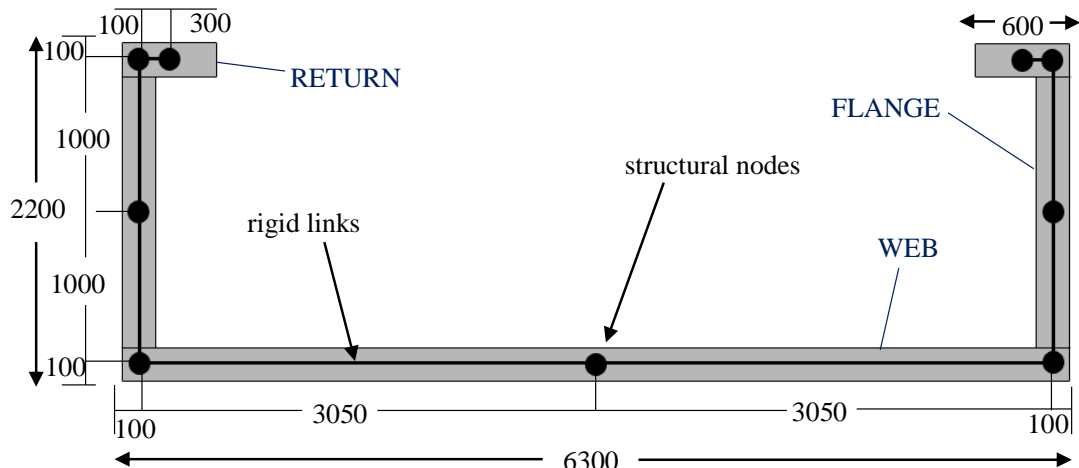
FIGURE 11: RIGID HORIZONTAL LINKS IMPOSED ON C-SHAPED WALL (MR) IN SEISMOSTRUCT

The bilinear steel model was used for the material modelling in representing the stress-strain behaviour of the steel. Inputs for this material model include modulus of elasticity (E_s = 200GPa), yield strength (f_{sy} = 551 MPa), strain hardening parameter (e_{sh} = 0.01) and fracture/buckling strain (e_{su} = 0.05), based on the mean values for the D500N steel bars tested by Menegon et al. [52]. Note that there is no input for the ultimate strength of the steel reinforcement (f_{su}), which instead is calculated based on the ε_{sh} value used (and an assumed bilinear shape). The trilinear concrete model was used to represent the stress-strain relationship of the concrete based on Popovics [66] NSC values. A mean compressive strength (f_{cmi}) of 40 MPa was assumed, with an initial stiffness of 20 GPa and residual strength of 8 MPa.

The wall elements were linked with a rigid diaphragm in SeismoStruct to allow mid-rise buildings to deform appropriately, with the floors on each level being held rigid in the x-y plane but allowing out-of-plane deformations. Nodes placed central to the floor plan at each level were used as the "master node" for the rigid diaphragm constraint, but also allowed the total floor mass of the building to be lumped at the center (Figure 12). The assumption of the center of mass was used such that the effects of torsional response of the building would be neglected. The total floor mass, using the dead load (G) and live load (Q) values

in Table 9, were calculated using the seismic mass combination of G + 0.3Q in accordance with AS 1170.0:2002 [67]. Excluding the mass of the axial load, which was subjected on the walls separately, the resulting lumped building masses corresponded to 50.35 tonnes (493.93 kN) and 563.84 tonnes (5531.32 kN) per floor for the rectangular and C-shaped wall buildings respectively.
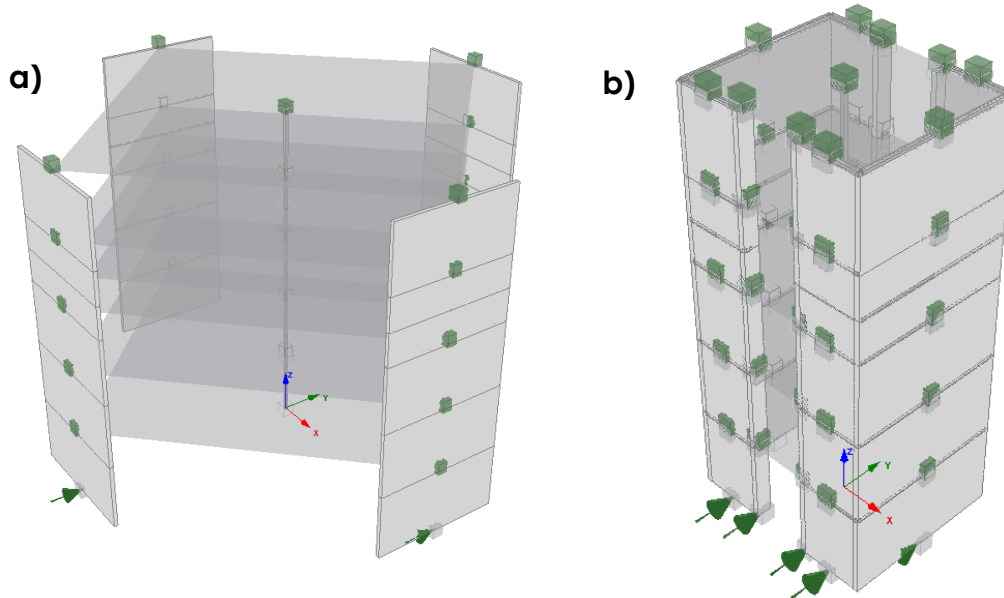

FIGURE 12 SEISMOSTRUCT MODELS FOR (A) RECTANGULAR (PERIPHERAL) WALL BUILDING AND (B) C-SHAPED WALL BUILDING

An nelastic truss element was used for the central truss to avoid instability problems while running the NDTHA. An elastic material model (el_mat) was used for the behaviour of the central truss, with a modulus of elasticity of 1 kPa. The elastic material also has a specific weight of 0 kN/m^3. Furthermore, the central structural nodes that make up the truss are restrained from movement in the z-direction, such that the nodes do not deform vertically due to the lumped masses being applied.

Each of the time-histories are applied as an acceleration to all nodes at the base of the wall and central truss, with a "curve multiplier" value of 9.81 such that the acceleration is applied in m/s^2. The time step output from SeismoArtif of all acceleration time-history files was 0.01 s.

Comparison between CSM and NDTHA

The fragility function results for the three different performance levels are illustrated in Figure 13 for the two different methods; MATLAB in the legend corresponds to the results using the CSM, whereas SS are the results using SeismoStruct and NDTHA. The results of the functions using the two different methods compare well, particularly for the slight damage (Serviceability) and moderate damage (Damage Control) performance limits in Figure 13(a) and (b). The median *PGA* determined from the results of both methods are similar for the extensive damage (Life Safety) performance level in Figure 13(c), but the overall fragility functions vary slightly due to the difference in the calculated standard deviation. The small difference in *β* values for the extensive damage performance level was found to be a result of the small number of ground motions (only 2) that were estimated to cause building number 3 to reach or exceed the extensive damage level using the NDTHA (SS) method for a *PGA* of

0.9g or 1.0g. In contrast, the CS (MATLAB) method estimated that all six ADRS used caused the building to reach or exceed this performance level with a *PGA* 0.9g and beyond. This was caused by the variance in the earthquake demand, which could also affect the resulting fragility functions. However, the two fragility functions do not drastically differ. It is expected that with a larger dataset, the standard deviations calculated from the two methods would be reduced and thus the fragility functions would converge.
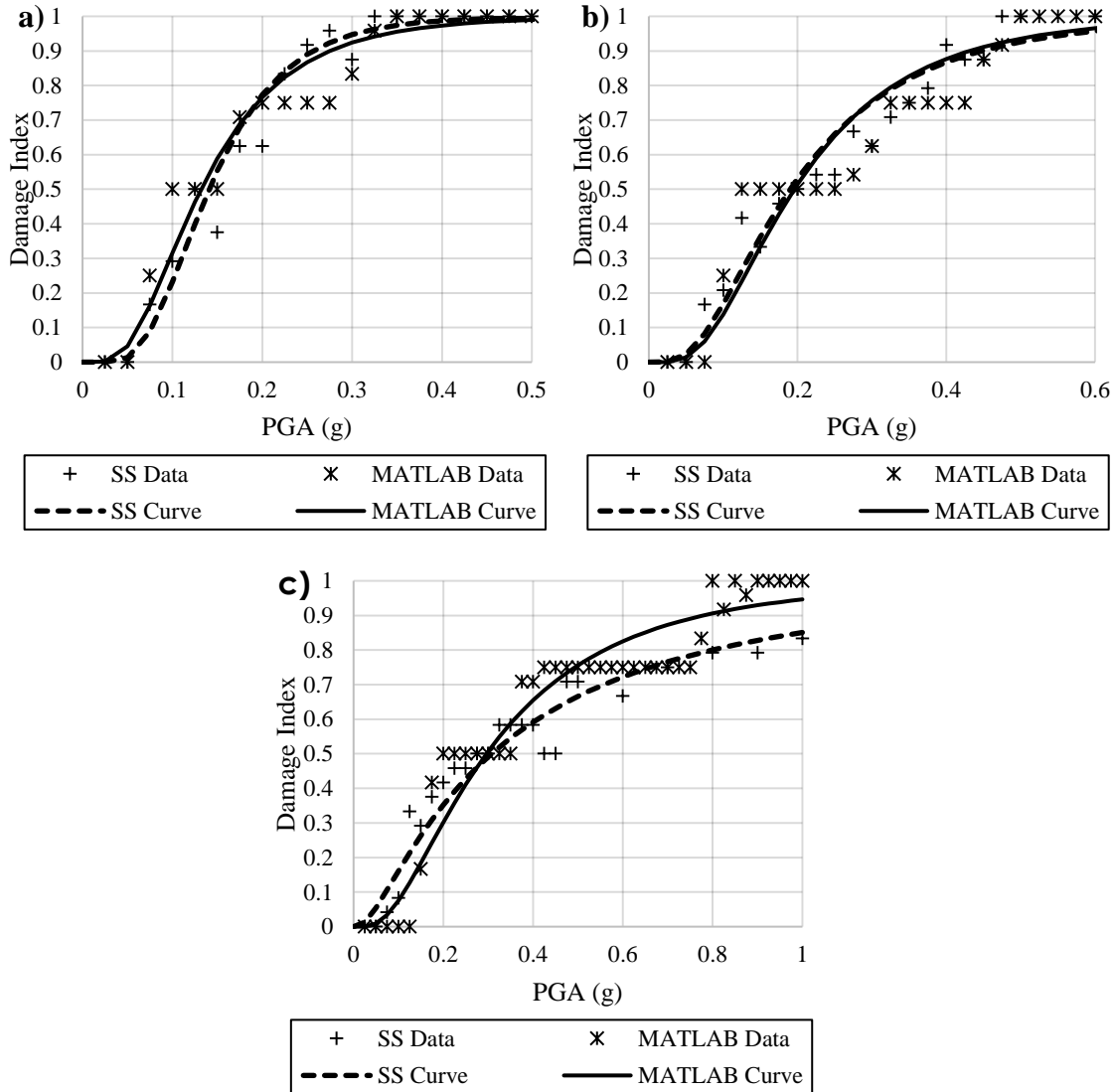

FIGURE 13 SEISMOSTRUCT (SS) AND MATLAB FRAGILITY FUNCTION RESULTS FOR (A) SERVICEABILITY (B) DAMAGE CONTROL AND (C) COLLAPSE PREVENTION

RC frames buildings

Fragility curves for the RC frames buildings will be conducted using nonlinear dynamic time history analysis (NDTHA). The nonlinear models for the three archetype buildings are created in the finite element analysis package OpenSEES [68].

Uniaxial material models need to be assigned to describe the load-deformation response of the concrete and steel fibres. In this study the concrete fibres are modelled using the Popovics [66] uniaxial concrete stress-strain material model which is available in OpenSees as *Concrete04* and the reinforcement bars are

modelled using the Giuffré-Menegotto-Pinto uniaxial material model [69] which is available as *Steel02* model in OpenSEES. The material properties are based on the reported values from the experiments and are presented in Table 15.

Input parameter	Unconfined concrete	Confined concrete
Concrete compressive strength	f_c	Confined concrete compressive strength: $f_{cc} = K f_c$ where K is the confinement factor according to Mander et al. [70]
Strain at maximum strength	$\varepsilon_{c0} = 0.002$	$\varepsilon_{cc0} = \varepsilon_{c0}(1 + 5(K-1))$ [70]
Strain at crushing strain	$\varepsilon_{cu} = 0.012 - 0.0001 f_c$ [71]	$\varepsilon_{ccu} = 5\varepsilon_{cc0} + 0.004$ [71]
Initial stiffness	$E = 5000\sqrt{f_c}$	$E = 5000\sqrt{f_c}$
Maximum tensile strength	$f_{ct} = 0.6\sqrt{f_c}$ (As 3600: 2009)	$f_{ct} = 0.6\sqrt{f_c}$ (As 3600: 2009)
Ultimate tensile strain	$\varepsilon_t = 0.1\varepsilon_{cu}$	$\varepsilon_t = 0.1\varepsilon_{cu}$

TABLE 15: INPUT PARAMETERS ADOPTED FOR CONCRETE04 MATERIAL MODEL FOR EVALUATING DIFFERENT MODELLING APPROACHES

The columns, beams, and walls are modelled using lumped plasticity elements and the beam-column joint response is modelled using the scissor's model with rigid links approach. As an example, the schematic of the modeling method for the 5-storey building with plan symmetry is shown in Figure 12. It is assumed that the walls and the columns are fixed to the ground. Furthermore a rigid diaphragm assumption is also adopted. The backbone adopted for the analyses for columns and walls are presented in Figure 13. The definition of the critical points for assessment is provided in Table 16. *Pinching4* material model has been adopted to define the hysteretic behaviour. The values of the parameters defining the model were determined by calibration to experimental results published in the literature. Details can be found in Amirsardari et al. [72].

Damping is incorporated by using Rayleigh damping model with the tangent stiffness proportional damping constant calibrated to provide 5 % equivalent viscous damping ratio for the first fundamental elastic mode.
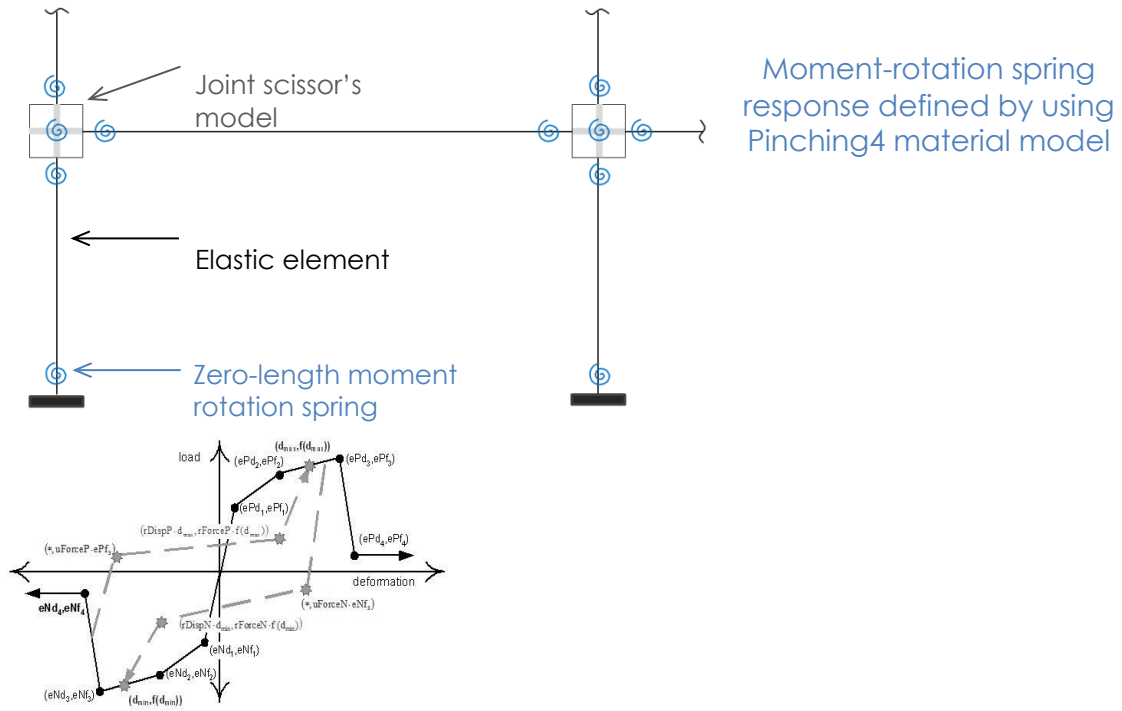
Elevation alona v-axis

Rigid links used to connect the frame to the centroid of the core walls

Elevation alona x-axis
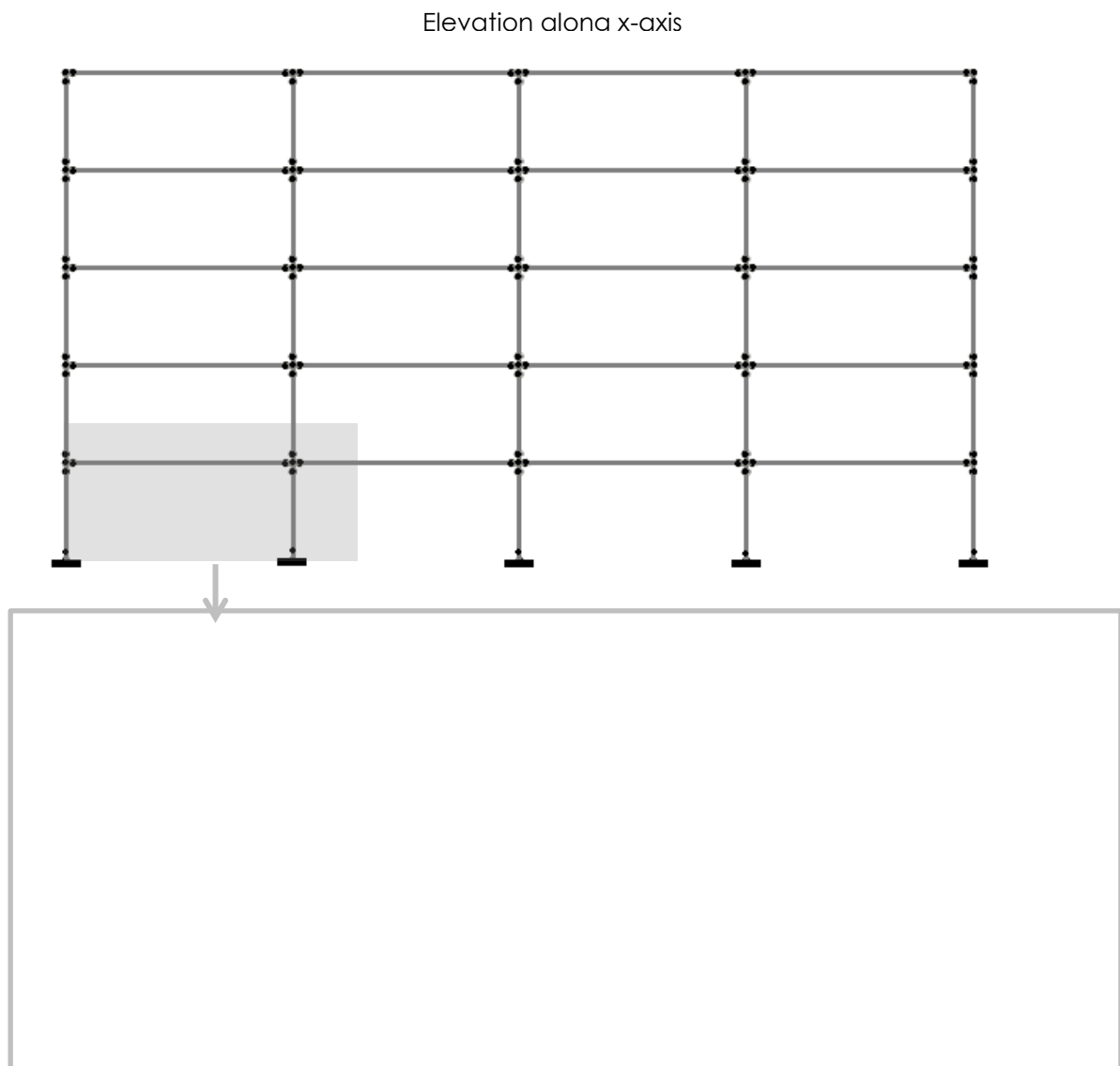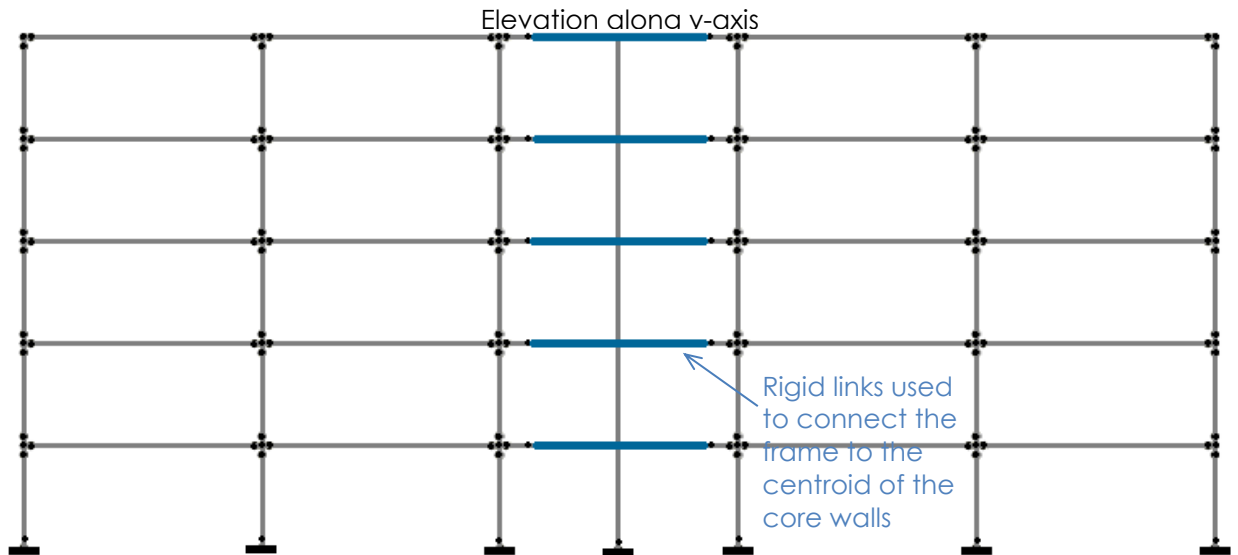
FIGURE 12: SCHEMATIC OF NONLINEAR BUILDING MODEL (EXAMPLE FOR 5-STOREY BUILDING WITH SYMMETRIC PLAN)

(a)

(b)
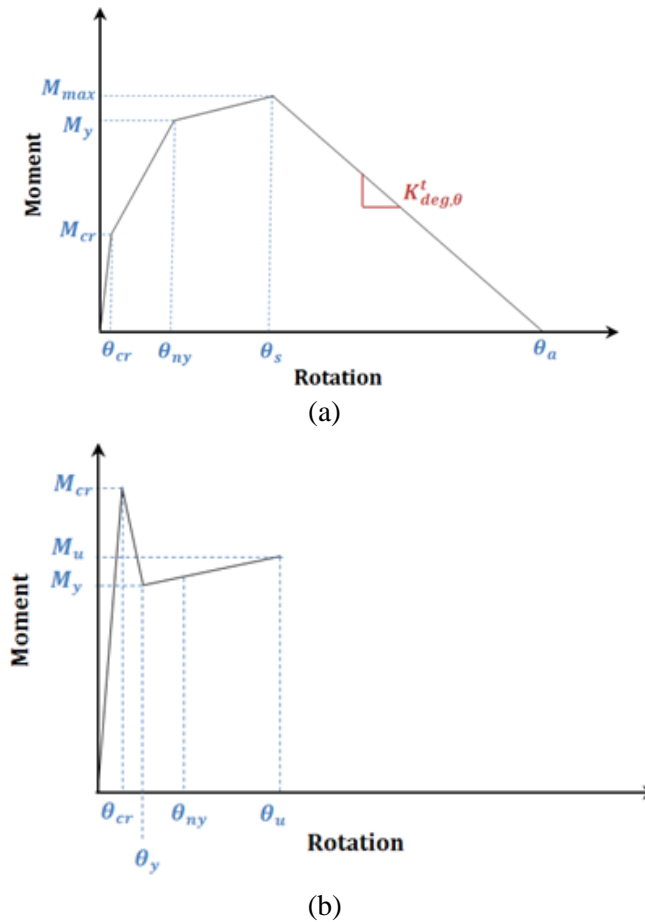
FIGURE 13: COMPONENT CACKBONE CURVE ADOPTED FOR THE ASSESSMENT: (A) COLUMNS, (B) WALL

Critical point	Criteria
Cracking Moment	For walls: the extreme tensile concrete fibre stress equals the flexural tensile strength of concrete (f_{ct}); $f_{ct} = 0.6\sqrt{f_c}$ based on Cook et al. [38] recommendation. For frame elements: the extreme tensile concrete fibre stress equals to zero.
Yield Moment	The extreme tensile steel fibre stress equals to the yield strength (f_y), or when the extreme compressive concrete fibre strain is equal to 0.002, depending on whichever occurs first as suggested by Priestley et al. [17].
Nominal Yield Moment	The extreme tensile steel fibre strain equals to 0.015, or when the extreme compressive concrete fibre strain equals to 0.003, depending on whichever occurs first as suggested by Priestley et al. [17]. The curvature at nominal yield is then calculated; $\phi_{ny} = \dfrac{M_N}{M_y}\phi_y$
Ultimate Moment	Is the point at which maximum moment is observed but it is limited to the following conditions, depending on whichever one occurs first; when the extreme tensile steel fibre strain equals to $0.6\varepsilon_{su}$, or when the extreme compressive concrete fibre strain equals to 0.004.

TABLE 16: DEFINITION OF CRITICAL POINTS FOR DEFINING COMPONENT BACKBONES

FRAGILITY CURVES

RC WALL BUILDINGS

The fragility curves for archetype low-rise LR, mid-rise MR and high-rise HR RC shear wall buildings are illustrated in Figures 14, 15 and 16, respectively. These figures show the expected Damage Index (probability of reaching or exceeding a given performance level) as a function of the intensity of the earthquake event, where *PGV* and Modified Mercalli Intensity (MMI) have been used as the *IM*. The *PGV* was converted to MMI using Equation (28) from Newmark and Rosenblueth [73]. Table 17 provides the resulting median (θ) and standard deviation (β) parameters for the vulnerability functions derived from the MATLAB assessment program.

$$2^I = \left(\frac{7}{5}\right) PGV \tag{28}$$

In 2014, Geoscience Australia (GA) released a report of the southeast Asian regional workshop on structural vulnerability models for the Global Risk Assessment ("GAR15") project [49]. This report includes vulnerability curves for several different classifications of structures subjected to earthquakes. The vulnerability curves for LR, MR and HR RC shear wall low resistance buildings have been superimposed in Figures 14 to 16. It should be noted that "low resistance" buildings, as classified in Maqsood *et al*. [49], are 'compatible with low local seismicity with a bedrock *PGA* <=0.1g with increasing variability of performance in an urban population of buildings'. The range of PGA is within the peak ground acceleration values currently used to design buildings of "normal importance" in accordance with the building's classification in [74] in all capital cities throughout Australia (AS1170.4:2007). If one reasonably assumes that the curves from Maqsood *et al*. [49] represent an "extensive damage" performance level, then the vulnerability functions derived from the research conducted here indicates a more vulnerable RC shear wall building stock for lower intensity earthquake events (e.g. *PGV* < 150 – 200 mm/s) in comparison to the curves from Maqsood *et al*. [49]. This observation is particularly true for the LR and MR buildings.
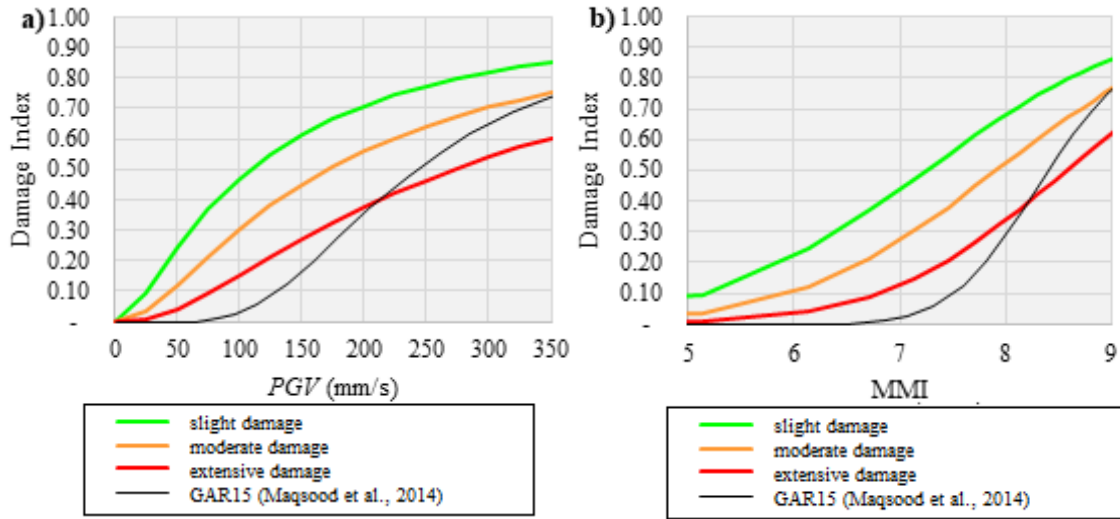
FIGURE 14 VULNERABILITY FUNCTIONS FOR LR RC STRUCTURAL WALL BUILDINGS FOR AN INTENSITY MEASURE OF (A) *PGV* AND (B) MMI
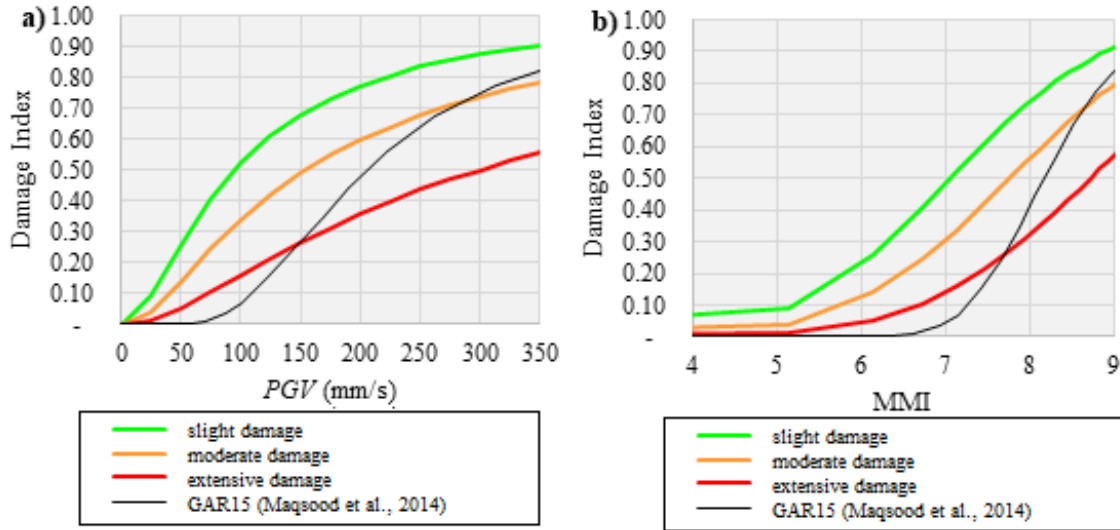

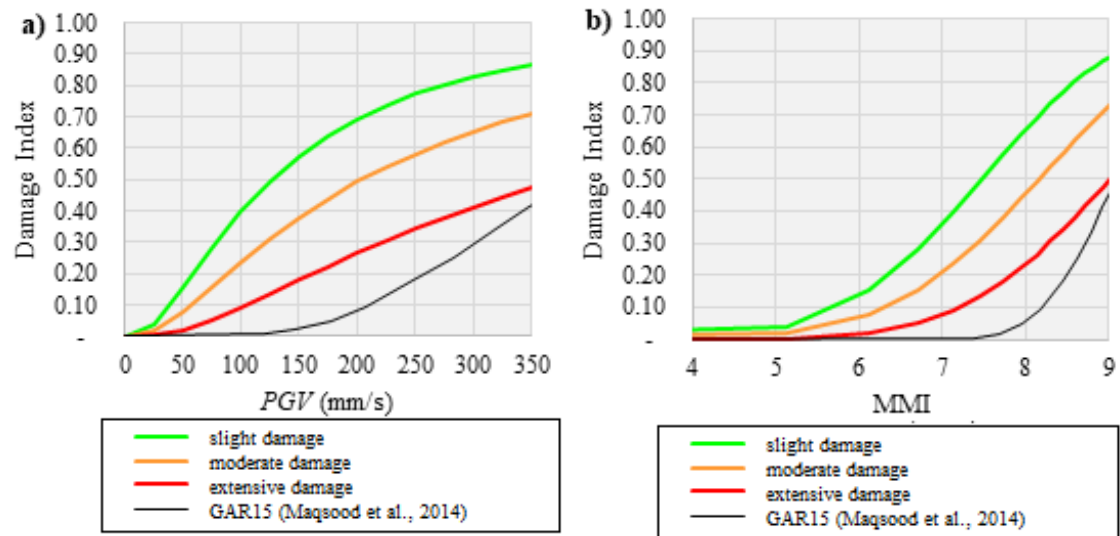FIGURE 15 VULNERABILITY FUNCTIONS FOR MR RC STRUCTURAL WALL BUILDINGS FOR AN INTENSITY MEASURE OF (A) *PGV* AND (B) MMI

FIGURE 16 VULNERABILITY FUNCTIONS FOR HR RC STRUCTURAL WALL BUILDINGS FOR AN INTENSITY MEASURE OF (A) PGV AND (B) MMI

	Serviceability		Damage Control		Collapse Prevention	
	Θ	*β*	*Θ*	*β*	*Θ*	*β*
LR	108.4	1.11	171.8	1.04	272.4	0.96
MR	94.9	1.00	154.4	1.05	299.8	1.10
HR	126.8	0.91	204.1	0.98	373.3	0.99

TABLE 17 MEDIAN (*Θ*) AND STANDARD DEVIATION (*B*) VALUES FOR FRAGILITY CURVES (WHERE *IM = PGV*)

RC FRAMES BUILDINGS

The parameters used for the constructions of fragility curves of RC frames buildings are PGV and RSD_{max}, since they consistently provide the lowest dispersion between the IM and structural response of the buildings analysed. However, for the purpose of comparison, fragility curves will also be developed using the conventional IM, PGA.

The probabilistic seismic demand models using the cloud analysis method are provided for when the intensity measure is PGA, PGV and RSD_{max}, for the 2-, 5- and 9-storey buildings in Figures 17 to 25. The corresponding fragility curves are provided in Figures 26 to 28. The fragility curves represented with a solid line are computed by only considering the dispersion due to the critical demand-to-capacity ratio as a function of IM for non-*collapse* data ($\beta_{Y|IM,\bar{c}}$), the fragility curves represented with a broken line are computed by considering $\beta_{Y|IM,\bar{c}}$ and dispersion due to uncertainty in defining the capacity of the building (β_C) and modelling uncertainties (β_M), which are set to 0.3 and 0.2, respectively. The difference between not considering and considering β_C and β_M to compute the fragilities is greater for the performance levels corresponding to higher level of damage, namely Extensive damage (*Life Safety*) and Complete damage (*Collapse Prevention*). This is because $\beta_{Y|IM,\bar{c}}$ is lower for these performance levels, thus adding β_C and β_M has more of an effect on the shape of the fragility curves. Furthermore, the fragilities computed for the performance levels corresponding to lower levels of damage, have higher probability of exceedance at lower intensity measures, therefore the increase in uncertainty has a lower effect on the shape of the fragilities. Hence, it may be concluded that the consideration of uncertainties becomes particularly important for performance levels corresponding higher levels of damage.

The results illustrate that there is a significant difference between the capacity of the buildings at Extensive damage and Complete damage, especially as the height of the buildings increases. The structural damage limits at these two performance levels were defined to correspond to the initiation of loss of lateral load carrying capacity and loss of axial load carrying capacity, respectively. The loss of lateral load carrying capacity is predominantly governed by the response of the core walls. The loss of axial load carrying capacity is predominantly governed by failure of the ground level columns since as the core wall start to lose their stiffness the lateral load is resisted by the gravity frames. Hence, the results show that collapse of gravity system does not occur prior to the ultimate capacity of the core walls is reached.

Furthermore, to provide an indication of the performance of the buildings, the intensity measures corresponding to a 500 and 2500 YRP event in accordance to AS 1170.4:2007 are shaded on Figures 26 to 28. By looking at the extreme ends of

the shaded regions (which represent the IM on Class A and Class E) it is apparent that the probability of exceedance for the various performance levels varies depending on the selected intensity measure. This is an interesting observation, as it is illustrates that different conclusions could potentially be derived for the same building depending on the IM selected to plot the fragility curves. The largest difference in the computed probability of exceedance is apparent when PGA instead of PGV or RSD_{max} is used as the IM. This is because PGA is a not a good IM to represent the varying levels of ground shaking caused by earthquakes. It is particularly not a good IM to incorporate the effects of local site conditions, especially if the current method in AS 1170.4:2007 is adopted.
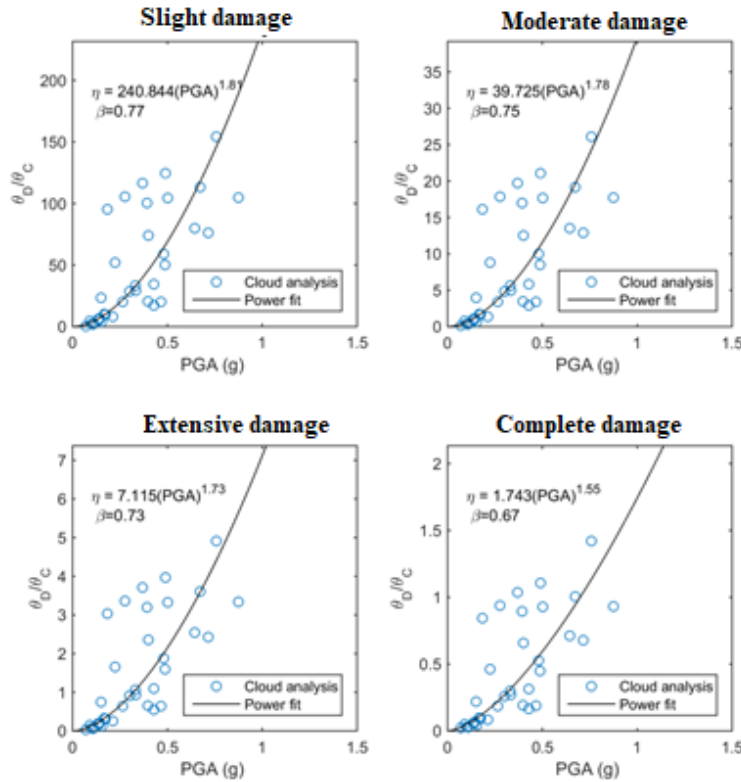
FIGURE 17: PSDM FOR 2-STOREY SYMMETRIC BUILDING WITH PGA AS THE IM
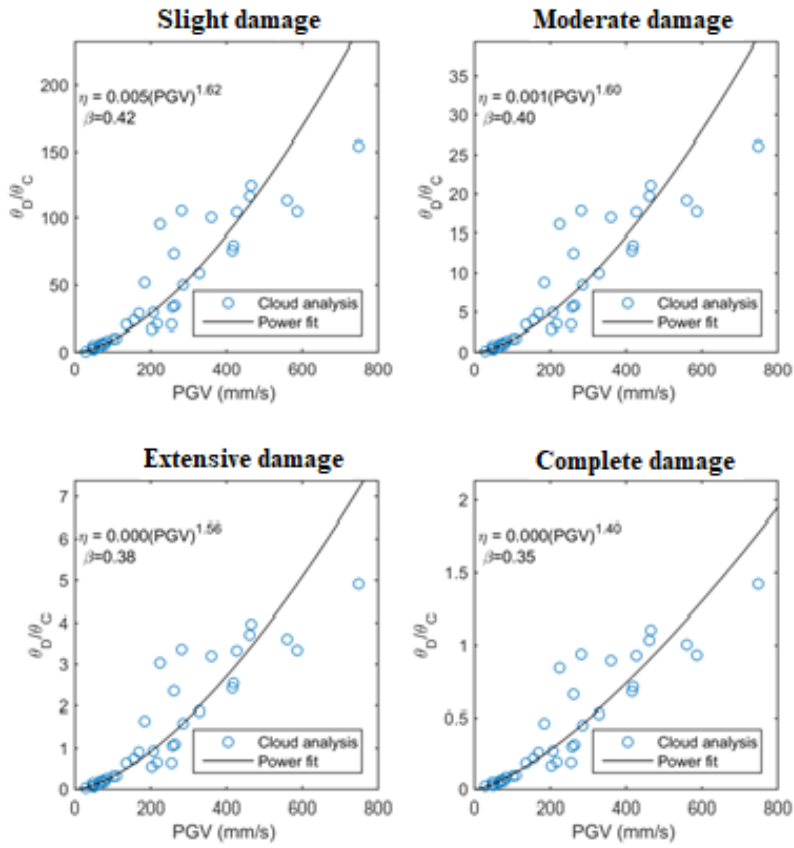
FIGURE 18: PSDM FOR 2-STOREY SYMMETRIC BUILDING WITH PGV AS THE IM
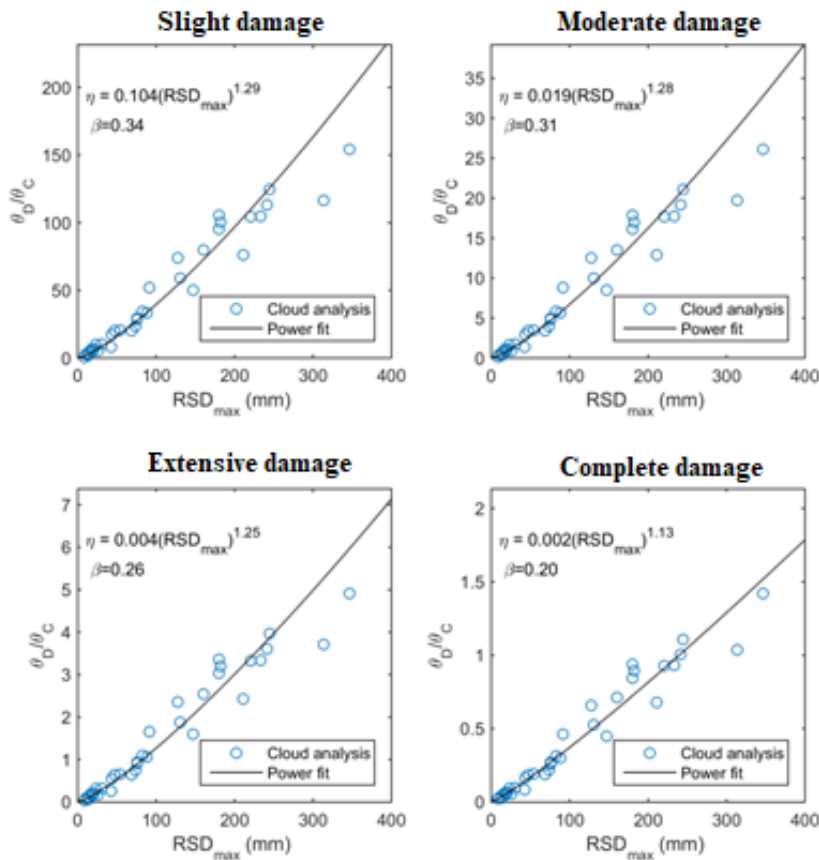
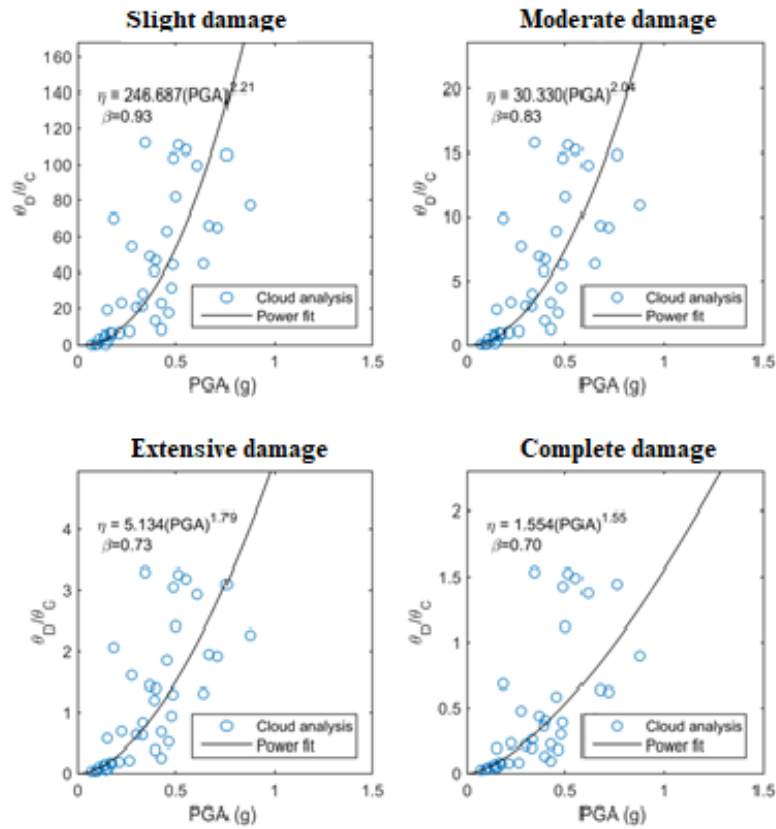FIGURE 19: PSDM FOR 2-STOREY SYMMETRIC BUILDING WITH RSDMAX AS THE IM

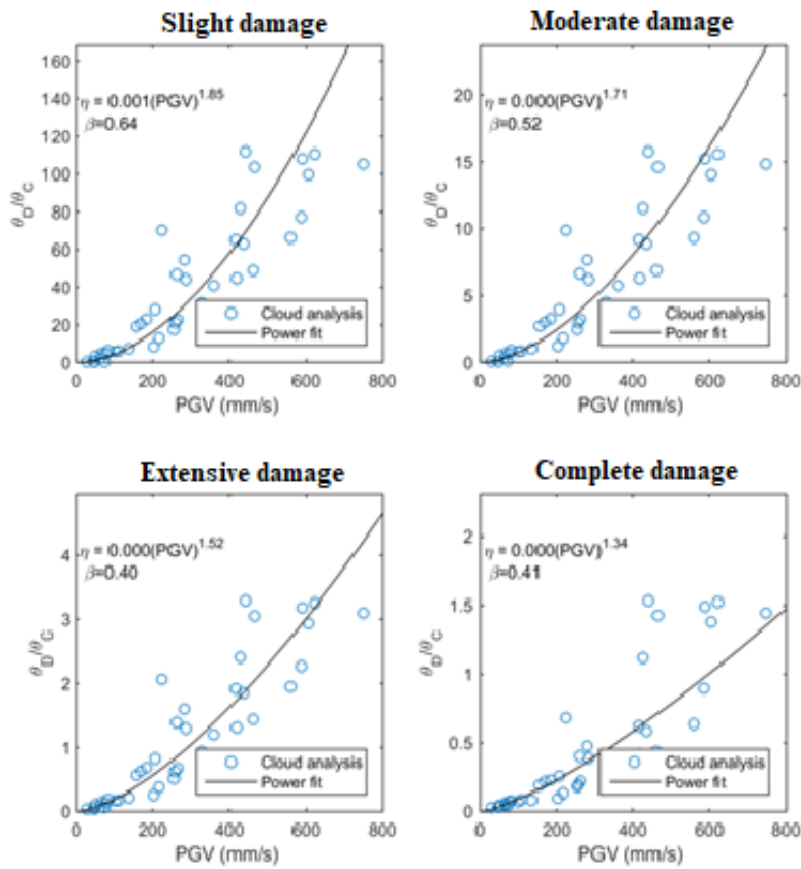FIGURE 20: PSDM FOR 5-STOREY SYMMETRIC BUILDING WITH PGA AS THE IM

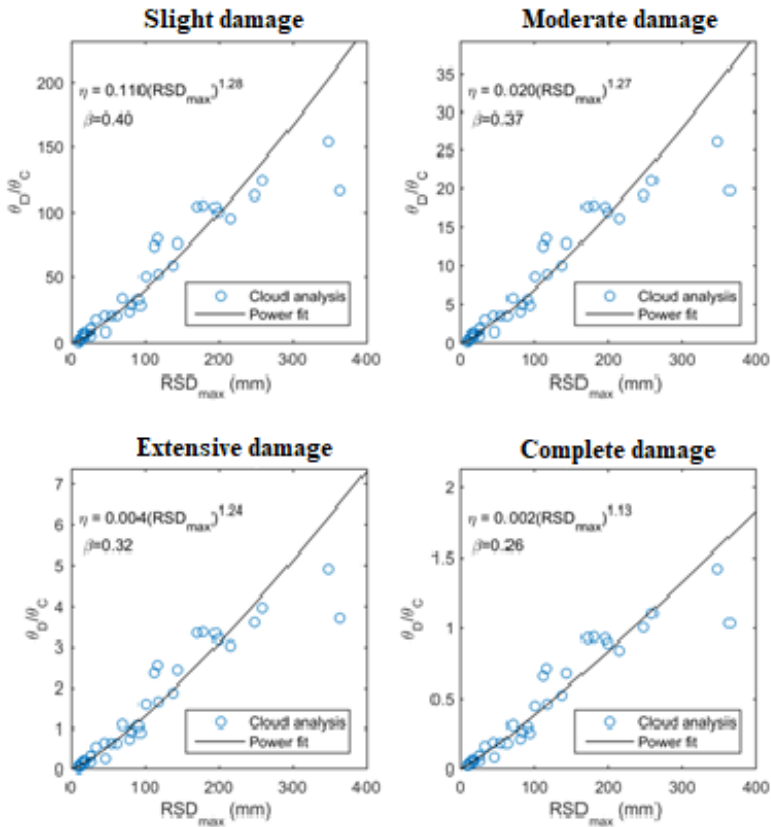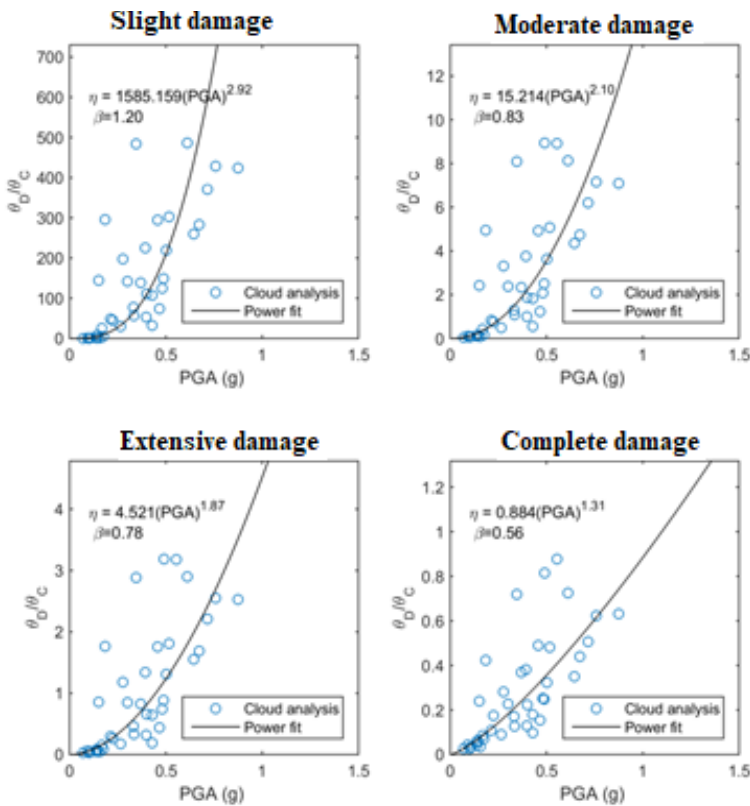FIGURE 21: PSDM FOR 5-STOREY SYMMETRIC BUILDING WITH PGV AS THE IM

FIGURE 22: PSDM FOR 5-STOREY SYMMETRIC BUILDING WITH RSD$_{MAX}$ AS THE IM

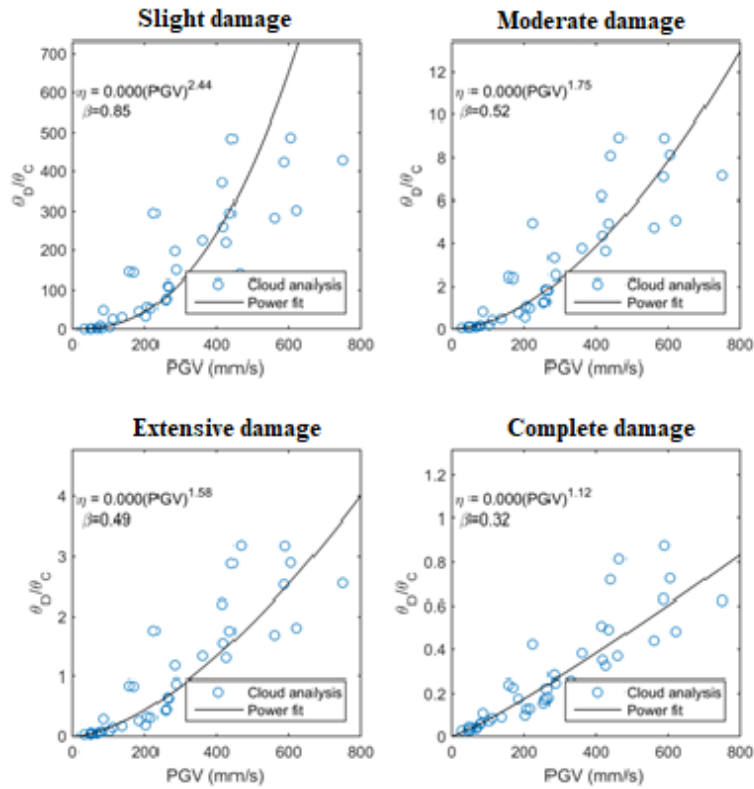FIGURE 23: PSDM FOR 9-STOREY SYMMETRIC BUILDING WITH PGA AS THE IM

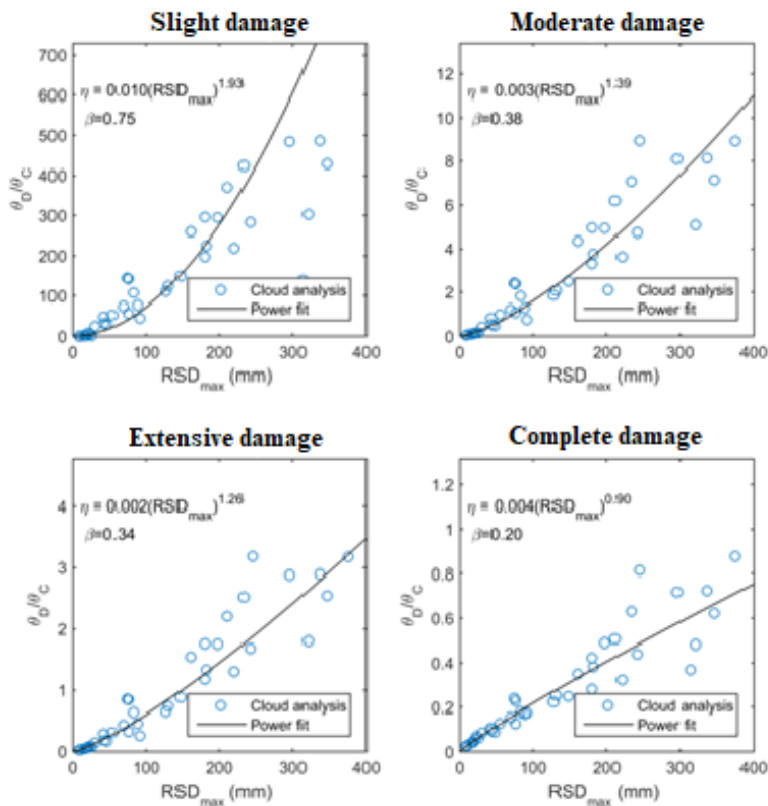FIGURE 24: PSDM FOR 9-STOREY SYMMETRIC BUILDING WITH PGV AS THE IM

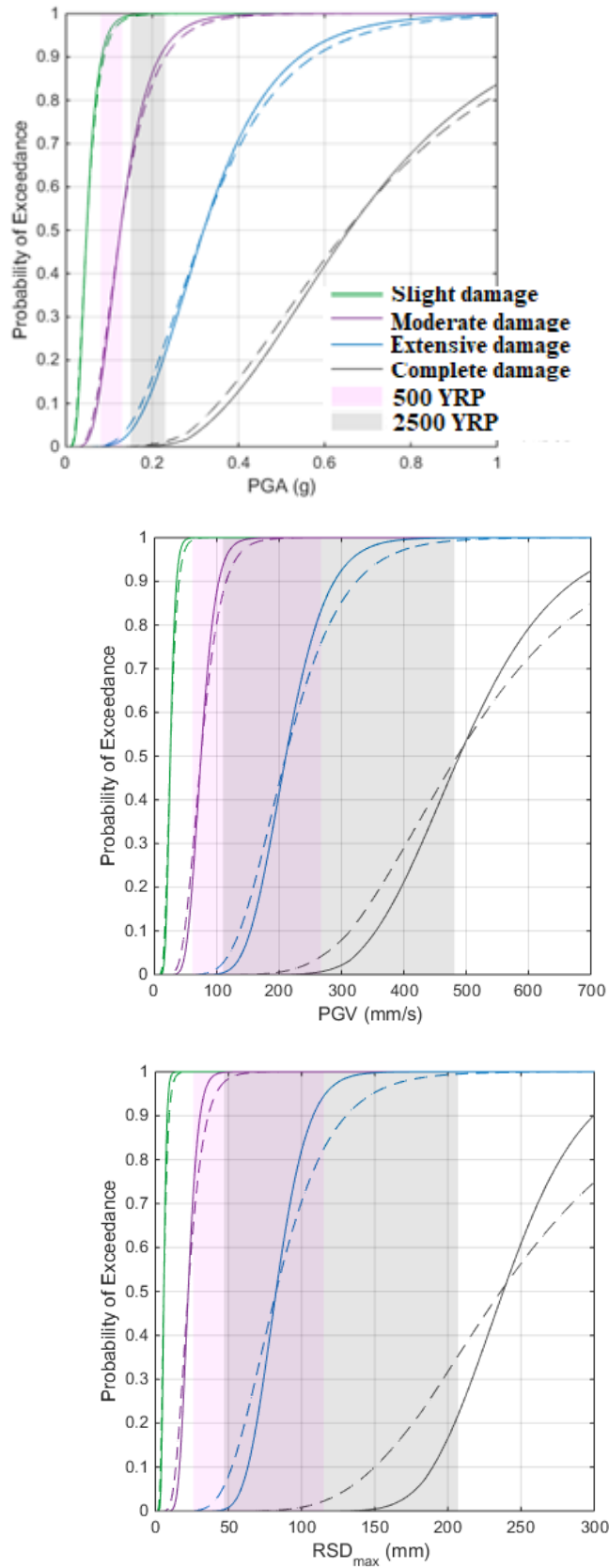FIGURE 25: PSDM FOR 9-STOREY SYMMETRIC BUILDING WITH RSDMAX AS THE IM

FIGURE 26: FRAGILITY CURVES FOR 2-STOREY BUILDING, USING PGA, PGV AND RSD$_{MAX}$ AS IM, SOLID LINE: ONLY $\beta_{Y|IM,\hat{\varepsilon}}$ IS CONSIDERED, BROKEN LINE: $\beta_{Y|IM,\hat{\varepsilon}}$, β_C AND β_M ARE CONSIDERED

FIGURE 27: FRAGILITY CURVES FOR 5-STOREY BUILDING, USING PGA, PGV AND RSD$_{MAX}$ AS IM, SOLID LINE: ONLY $\beta_{Y|IM,\hat{\varepsilon}}$ IS CONSIDERED, BROKEN LINE: $\beta_{Y|IM,\hat{\varepsilon}}$, β_C AND β_M ARE CONSIDERED
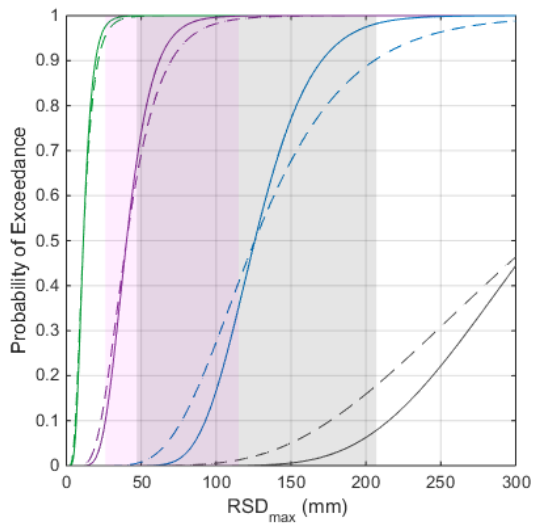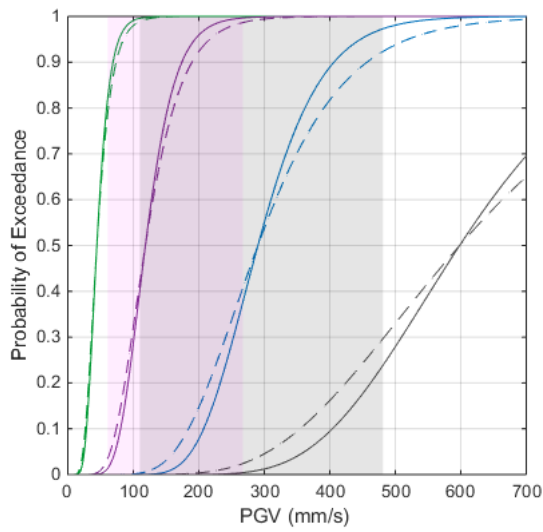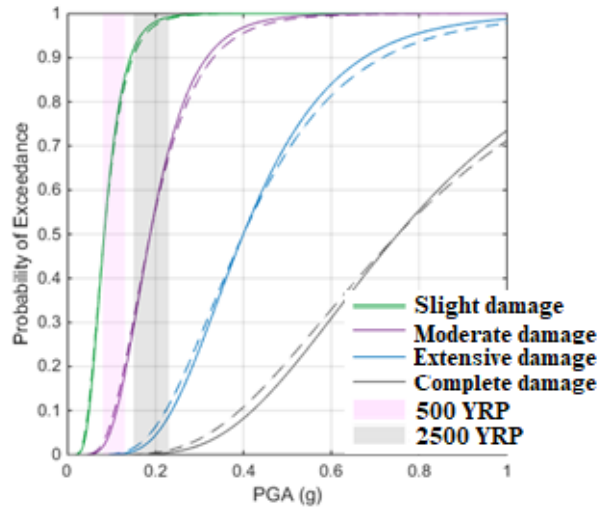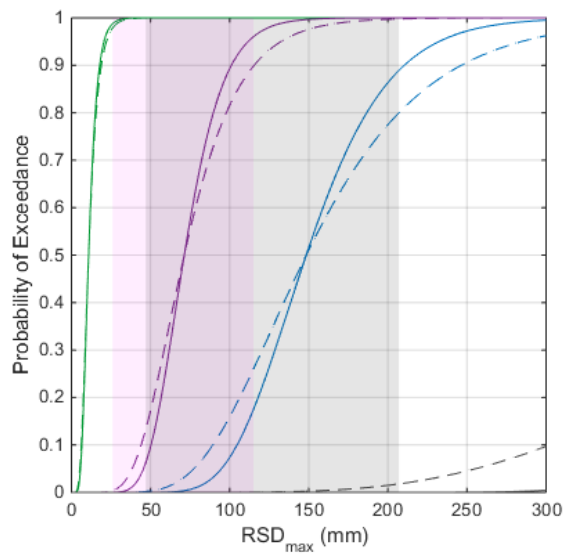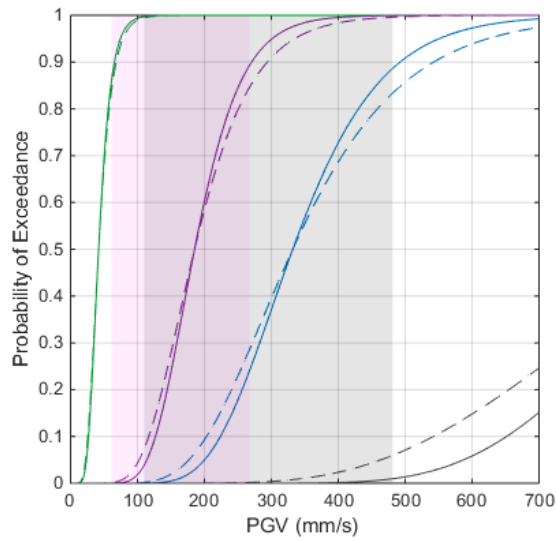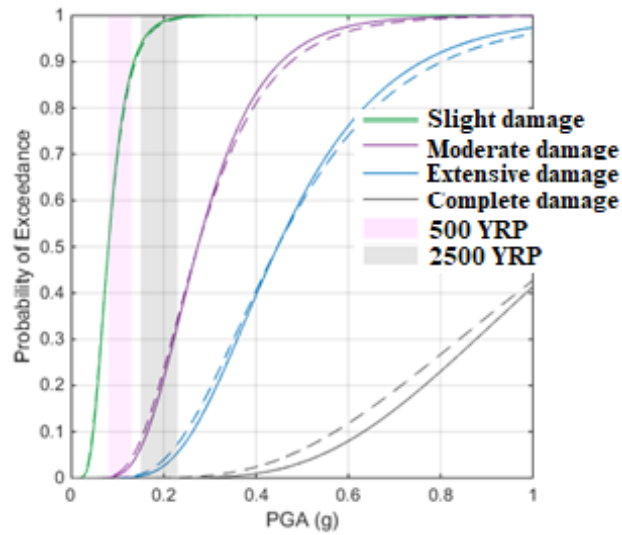
FIGURE 28: FRAGILITY CURVES FOR 5-STOREY BUILDING, USING PGA, PGV AND RSD$_{MAX}$ AS IM, SOLID LINE: ONLY $\beta_{Y|IM,\hat{c}}$ IS CONSIDERED, BROKEN LINE: $\beta_{Y|IM,\hat{c}}$, β_C AND β_M ARE CONSIDERED

CONCLUDING REMARKS

This report presents sets of fragility curves for limited ductile reinforced concrete buildings. Fragility curves were presented for limited-ductile reinforced concrete (RC) buildings typical of Australian constructions: i) fragility curves for RC buildings that are primarily supported by limited-ductile RC shear wall (referred to **RC shear walls buildings** in this report); ii) fragility curves for RC buildings that are supported by limited-ductile RC walls and frames (referred to **RC frames buildings** in this report). A detailed description of the framework adopted to assess the seismic performance of archetype buildings has been presented.

The assessment is conducted by performing nonlinear analyses using the capacity spectrum method and time history analyses of the 3D nonlinear building models, for RC shear walls and RC frames buildings respectively. Ground motion records have been selected from a combination of stochastically generated records, historical records with characteristics representative of Australian earthquakes and simulated records on soil conditions. The multi-stripe and cloud analyses have been adopted to compute the fragility functions. The fragility curves for low-rise, mid-rise and high-rise buildings for both types of limited ductile reinforced concrete buildings have been presented in the forms of PGV, MMI and RSD_{max} as intensity measures.

It should be noted that the information presented in this report are based on the up to date knowledge of the project team. It is noted that there are ongoing works on this topic, being carried by in conjunction with PhD students who are financially supported by this BNHCRC project.

REFERENCES

1 Liel, A.B., Deierlein, G.G., 2013. Cost-benefit evaluation of seismic risk mitigation alternatives for older concrete frame buildings. Earthquake Spectra 29(4), 1391-1411.

2 Porter, K. (2016). A beginner's guide to fragility, vulnerability, and risk (pp. 92). Denver CO, USA: University of Colorado Boulder.

3 Baker, J. W. (2015). Efficient analytical fragility function fitting using dynamic structural analysis. *Earthquake Spectra, 31*(1), 579-599. doi: 10.1193/

4 Celik, O. C. (2007). *Probabilistic assessment of non-ductile reinforced concrete frames susceptible to mid-America ground motions.* (PhD Thesis), Georgia Institute of Technology.

5 Jeon, J.-S., Lowes, L. N., DesRoches, R., & Brilakis, I. (2015). Fragility curves for non-ductile reinforced concrete frames that exhibit different component response mechanisms. *Engineering Structures, 85*, 127-143. doi: 10.1016/j.engstruct.2014.12.009

6 Nazari, Y. R. (2017). *Seismic fragility analysis of reinforced concrete shear wall buildings in Canada.* (PhD thesis), University of Ottawa, Canada

7 Seo, J., Hu, J., & Davaajamts, B. (2015). Seismic Performance Evaluation of Multistory Reinforced Concrete Moment Resisting Frame Structure with Shear Walls. *Sustainability, 7*(10), 14287-14308. doi: 10.3390/su71014287

8 Applied Technology Council. (2012). Seismic performance assessment of buildings (FEMA P-58) *Volume 1: Methodology*. Washington, D.C: Federal Emergency Management Agency.

9 Vamvatsikos, D., & Cornell, C. A. (2002). Incremental dynamic analysis. *Earthquake Engineering & Structural Dynamics, 31*(3), 491-514. doi: 10.1002/eqe.141

10 Jalayer, F., & Cornell, C. A. (2009). Alternative non-linear demand estimation methods for probability-based seismic assessments. *Earthquake Engineering & Structural Dynamics, 38*(8), 951-972. doi: 10.1002/eqe.876

11 Jalayer F (2003) Direct Probabilistic seismic analysis: implementing non-linear dynamic assessments. Ph.D. dissertation, Stanford University, California

12 Jalayer, F., Ebrahimian, H., Miano, A., Manfredi, G., & Sezen, H. (2017). Analytical fragility assessment using unscaled ground motion records. *Earthquake Engineering & Structural Dynamics*. doi: 10.1002/eqe.2922

13 Rajeev, P., Franchin, P., & Tesfamariam, S. (2014). *Probabilistic seismic demand model for RC frame buildings using cloud analysis and incremental dynamic analysis.* Paper presented at the Tenth U.S. National Conference on Earthquake Engineering (NCEE), Anchorage, Alaska.

14 Jalayer, F., De Risi, R., & Manfredi, G. (2014). Bayesian Cloud Analysis: efficient structural fragility assessment using linear regression. *Bulletin of Earthquake Engineering, 13*(4), 1183-1203. doi: 10.1007/s10518-014-9692-z

15 Cornell, C. A., Jalayer, F., Hamburger, R. O., & Foutch, D. A. (2002). Probabilistic basis for 2000 SAC Federal Emergency Management Agency steel moment frame guidelines. *Journal of Structural Engineering, 128*(8), 526-533. doi: 10.1061//ASCE/0733-9445/2002/128:4/526

16 Rajeev, P., Franchin, P., & Pinto, P. E. (2008). Increased accuracy of vector-IM-based seismic risk assessment? *Journal of Earthquake Engineering, 12*(sup1), 111-124. doi: 10.1080/13632460801925798

17 Priestley, M. J. N., Calvi, G. M., & Kowalsky, M. J. (2007). *Displacement-based seismic design of structures*. Pavia, Italy: IUSS Press.

18 American Society of Civil Engineers (ASCE/SEI). (2013). Seismic evaluation and retrofit of existing buildings. Reston, Virginia: American Society of Civil Engineers.

19 Sullivan, T. J., Priestley, M. J. N., & Calvi, G. M. (2012). *A model code for the displacement-based seismic design of structures*. Instituto Universitario di Studi Superiori di Pavia: IUSS Press.

20 Standards Australia. (2009). AS 3600-2009: Concrete Structures.

21 Standards New Zealand. (2004). NZS 1170.5:2004 Structural design actions - Part 5: earthquake actions - New Zealand. Wellington.

22 Standards Australia. (2007). AS 1170.4-2007: Structural design actions, Part 4: Earthquake actions in Australia. Sydney, NSW.

23 Standards Australia. (1993). AS 1170.4 Supplement 1-1993 *Minimum design loads on structures, Part 4: Earthquake loads - Commentary*. Sydney, NSW.

24 McBean, P. C. (2008). Drift intolerant facade systems and flexible shear walls: Do we have a problem. *Australian Journal of Structural Engineering, 8*(1), 77-84.

25 Baradaran Shoraka, M., Yang, T. Y., & Elwood, K. J. (2013). Seismic loss estimation of non-ductile reinforced concrete buildings. Earthquake Engineering & Structural Dynamics, 42(2), 297-310. doi: 10.1002/eqe.2213

26 Giovenale, P., Cornell, C. A., & Esteva, L. (2004). Comparing the adequacy of alternative ground motion intensity measures for the estimation of structural responses. Earthquake Engineering & Structural Dynamics, 33(8), 951-979. doi: 10.1002/eqe.386

27 Wilson, J., & Lam, N. (2007). AS 1170.4-2007 commentary: Structural design actions. Part 4, Earthquake actions in Australia. Victoria: Australian Earthquake Engineering Society: McKinnon.

28 Glaister, S., & Pinho, R. (2009). Development of a Simplified Deformation-Based Method for Seismic Vulnerability Assessment. Journal of Earthquake Engineering, 7(sup001), 107-140. doi: 10.1080/13632460309350475

29 Lam, N. T. K. (1999). GENQKE'' User's Guide: Program for generating synthetic earthquake accelerograms based on stochastic simulations of seismological models. Department of Civil and Environmental Engineering, The University of Melbourne, Australia.

30 Brown, A., & Gibson, G. (2004). A multi-tiered earthquake hazard model for Australia. *Tectonophysics, 390*(1–4), 25-43.

31 Ordonez, G. A. (2013). SHAKE2000 (Version 9.99.2 - July 2013). Retrieved from http://www.geomotions.com

32 Hashash, Y. M. A., Musgrove, M. I., Harmon, J. A., Groholski, D. R., Phillips, C. A., & Park, D. (2016). DEEPSOIL 6.1. Retrieved from http://deepsoil.cee.illinois.edu/

33 Kayen, R. E., Carkin, B. A., Allen, T., Collins, C., McPherson, A., & Minasian, D. (2015). Shear-wave velocity and site-amplification factors for 50 Australian sites determined by the spectral analysis of surface waves methods: U.S. Geological Survey Open-File Report 2014-1264, 118 p. doi: http://dx.doi.org/10.3133/ofr20141264

34 Kwon, O.-S., & Elnashai, A. (2006). The effect of material and ground motion uncertainty on the seismic vulnerability curves of RC structure. Engineering Structures, 28(2), 289-303. doi: 10.1016/j.engstruct.2005.07.010

35 Hyland. (2011). *Pyne Gould Corportation Building Site Examination and Materials Tests*. Retrieved from http://www.mbie.govt.nz/publications-research/research/building-and-construction/quake-pgc-site-and-materials-report.pdf/at_download/file

36 Smith, P., & England, V. (2012). *Independent Assessment on Earthquake Performance of Gallery Apartments - 62 Gloucester Street. Report prepared for the Canterbury Earthquakes Royal Commision*. Retrieved from http://canterbury.royalcommission.govt.nz/documents-by-key/20120217.3188

37 Moehle, J. (2015). *Seismic design of reinforced concrete buildings*. New York, N.Y.: McGraw-Hill Education LLC.

38 Cook, D., Fenwick, R., & Russell, A. (2014). Amendment 3 to NZS3101. Paper presented at the The New Zealand Concrete Industry Conference, Taupo, New Zealad.

39 NZSEE. (2016). The seismic assessment of existing buildings: technical guidelines for engineering assessments Revised draft 1- October 2016: Ministry of Business, Innovation and Employment, the Earthquake Commission, the New Zealand Society for Earthquake Engineering, the Structural Engineering Society and the New Zealand Geotechnical Society.

40 European Standard. (2004). Eurocode 2: Design of concrete structures - Part 1-2: General Rules - structural fire design EN 1992-1-2:2004. Brussels: European Committee for Standardization.

41 Foster, S. J., Stewart, M. G., Loo, M., Ahammed, M., & Sirivivatnanon, V. (2016). Calibration of Australian Standard AS3600 Concrete Structures: part I statistical analysis of material properties and model error. Australian Journal of Structural Engineering, 17(4), 242-253. doi: 10.1080/13287982.2016.1246793

42 Pham, L. (1985). Reliability analyses of reinforced concrete and composite column sections under concentric loads. *Institution of Engineers (Australia) Civ Eng Trans*, (1).

43 fib: féderation internationale du béton (International Federation for Structural Concrete). (2010). Model Code 2010, First complete draft Volume 1. Lausanne, Switzerland.

44 Menegon, S. J., Tsang, H. H., & Wilson, J. L. (2015). *Overstrength and ductility of limited ductile RC walls: from the design engineers perspective*. Paper presented at the Proceedings of the Tenth Pacific Conference on Earthquake Engineering, Sydney, Australia.

45 Standards Australia/New Zealand. (2001). AS/NZS 4671:2001 : Steel Reinforcing Materials.

46 Standards Australia. (1991). AS 1302:1991 Steel reinforcing bars for concrete.

47 FEMA. (2010). HAZUS MH MR5 Technical Manual. Washington, D.C.

48 Robinson, D., Fulford, G., & Dhu, T. (2005). EQRM: Geoscience Australia's Earthquake Risk Model. Technical Manual Version 3.0: Record 2005/01: Geoscience Australia: Canberra.

49 Maqsood, T., Wehner, M., Ryu, H., Edwards, M., Dale, K., & Miller, V. (2014). GAR15 Regional Vulnerability Functions *Record 2014/38*: Geoscience Australia: Canberra.

50 Henry, R. S. (2013). Assessment of the Minimum Vertical Reinforcement Limits for RC Walls. *Bulletin of the New Zealand Society for Earthquake Engineering, 46*(2), 88.

51 Albidah, A., Altheeb, A., Lam, N., & Wilson, J. (2013). *A Reconnaissance Survey on Shear Wall Characteristics in Regions of Low-to-Moderate Seismicity*. Paper presented at the Paper presented at the Australian Earthquake Engineering Society 2013 Conference, Hobart, Tasmania.

52 Menegon, S. J., Wilson, J. L., Lam, N. T. K., & Gad, E. F. (2017). RC walls in Australia: reconnaissance survey of industry and literature review of experimental testing. *Australian Journal of Structural Engineering, 18*(1), 24-40. doi:10.1080/13287982.2017.1315207

53 Hoult, R. (2017). *Seismic assessment of reinforced concrete walls in Australia*. (PhD), University of Melbourne. Retrieved from http://hdl.handle.net/11343/192443

54 Lam, N., Wilson, J., & Lumantarna, E. (2011). Force-deformation behaviour modelling of cracked reinforced concrete by EXCEL spreadsheets. *Computers and Concrete, 8*(1), 43-57.

55 Wong, P., Vecchio, F., & Trommels, H. (2013). Vector2 and FormWorks User Manual. Department of Civil Engineering, University of Toronto.

56 Seckin, M. (1981). *Hysteretic Behaviour of Cast-in-Place Exterior Beam-Column-Slab Subassemblies*. (Ph.D. Thesis), University of Toronto, Toronto, Canada.

57 Beyer, K. (2007). *Seismic design of torsionally eccentric buildings with U-shaped RC Walls*. (PhD), ROSE School. (ROSE-2008/0X)

58 Constantin, R. (2016). *Seismic behaviour and analysis of U-shaped RC walls*. École polytechnique fédérale de Lausanne, Lausanne, Switzerland.

59 Hoult, R., Goldsworthy, H., & Lumantarna, E. (2017). Displacement Capacity of Lightly Reinforced and Unconfined Concrete Structural Walls. *Manuscript submitted for publication*.

60 Priestley, M. J. N., Seible, F., & Calvi, G. M. (1996). *Seismic design and retrofit of bridges*: New York : Wiley, c1996.

61 Hoult, R., Goldsworthy, H., & Lumantarna, E. (2017). Plastic Hinge Length for Lightly Reinforced Rectangular Concrete Walls. *Journal of Earthquake Engineering*. doi:10.1080/13632469.2017.1286619

62 Seismosoft (2013). SeismoArtif - A computer program for generation of artificial accelerograms". Available from URL: www.seismosoft.com

63 Lam, N., Sinadinovski, C., Koo, R., Wilson, J. L., & Doherty, K. (2003). Peak ground velocity modelling for Australian intraplate earthquakes. *Journal of Seismology and Earthquake Engineering, 5*(2), 11-22.

64 Beyer, K., Dazio, A., & Priestley, M. J. N. (2008). Inelastic Wide-Column Models for U-Shaped Reinforced Concrete Walls. *Journal of Earthquake Engineering, 12*(sup1), 1-33. doi: 10.1080/13632460801922571

65 Seismosoft (2013). SeismoStruct v6.0 - Verification Report". Available from URL: www.seismosoft.com

66 Popovics, S. (1973). A numerical approach to the complete stress-strain curve of concrete. *Cement and concrete research*, *3*(5), 583-599.

67 Standards Australia and Standards New Zealand. (2002). AS/NSZ 1170.0-2002: Structural design actions, Part 0: General principles. Syndey, NSW, and Wellington.

68 McKenna, F., Fenves, G. L., Scott, M. N., & Jeremic, B. (2000). Open System for Earthquake Engineering Simulation (OpenSEES) (Version 2.4.5, 2013): Pacific Earthquake Engineering Research Center, University of California, Berkeley, CA. Retrieved from http://opensees.berkeley.edu/

69 Menegotto, M., & Pinto, P. E. (1973). *Method of analysis for cyclically loaded reinforced concrete plane frames including changes in geometry and non-elastic behavior of elements under combined normal force and bending.* Paper presented at the IABSE Sympoium on Resistance and Ultimate Deformability of Structures Acted on by Well-Defined Repeated Loads, International Association for Bridge and Structural Engineering, Zurich, Switzerland.

70 Mander, J. B., Priestley, M. J., & Park, R. (1988). Theoretical stress-strain model for confined concrete. *Journal of structural engineering*, *114*(8), 1804-1826.

71 Reddiar, M. K. M. (2009). *Stress-strain model of unconfined and confined concrete and stress-block parameters.* (Thesis), Office of Graduate Studies of Texas A&M University.

72 Amirsardari, A., Rajeev, P., Goldsworthy, H., Lumantarna, E. (2016). Modelling non-ductile reinforced concrete columns. Proceedings of the 2016 Australian Earthquake Engineering Society Conference, Melbourne, VIC

73 Newmark, N. M., & Rosenblueth, E. (1971). Fundamentals of earthquake engineering. *Civil engineering and engineering mechanics series, 12*.

74 ABCB. (2016). The National Construction Code (NCC) 2016 Buildings Code of Australia - Volume One: Australian Building Code Board (ABCB).